Planetary and Space Science 220 (2022) 105536

Contents lists available at ScienceDirect

Planetary and Space Science

journal homepage: www.elsevier.com/locate/pss

Impact ionization dust detection with compact, hollow and fluffy dust analogs

S. Hunziker [a,*], G. Moragas-Klostermeyer [b], J.K. Hillier [c], L.A. Fielding [d], K. Hornung [e], J.R. Lovett [f], S.P. Armes [f], J. Fontanese [g], D. James [g], H.W. Hsu [g], I. Herrmann [h,i], N. Fechler [j], O. Poch [k], A. Pommerol [l], R. Srama [m], D. Malaspina [n], V.J. Sterken [a]

[a] ETH Zürich, Department of Physics, Zürich, 8093, Switzerland
[b] University of Stuttgart, Institute of Space Systems, Stuttgart, 70569, Germany
[c] Freie Universität Berlin, Institute of Geological Sciences, Berlin, 12249, Germany
[d] The University of Manchester, Department of Materials and Henry Royce Institute, Manchester, M13 9PL, United Kingdom
[e] Universität der Bundeswehr München, LRT-7, Neubiberg, 85577, Germany
[f] University of Sheffield, Department of Chemistry, Sheffield, S3 7HF, United Kingdom
[g] University of Colorado, IMPACT-LASP, Boulder, 80303, USA
[h] ETH Zürich, Department of Mechanical and Process Engineering, Zürich, 8092, Switzerland
[i] Empa, Materials Meet Life, St. Gallen, 9014, Switzerland
[j] Max Planck Institute of Colloids and Interfaces, Potsdam, 14476, Germany
[k] Univ. Grenoble Alpes, Institut de Planétologie et d'Astrophysique de Grenoble (IPAG), Grenoble, 38000, France
[l] Universität Bern, Physikalisches Institut, Bern, 3012, Switzerland
[m] Universität Stuttgart, Institut für Raumfahrtsystme, Stuttgart, 70569, Germany
[n] University of Colorado, Astrophysical and Planetary Sciences Department, Boulder, 80305, USA

ARTICLE INFO

Keywords:
Cosmic dust
Impact ionization
High-velocity dust impacts

ABSTRACT

Impact ionization of high-velocity cosmic dust particles has been used as a basic principle for dust detectors in space for many decades. It has provided optimum means to gain insight into the dust environment in the solar system. The Ulysses Dust Detector System provided for the first time impact ionization-based detection of interstellar dust (ISD) in the solar system and discovered surprisingly heavy ISD particles with sizes up to a few microns. Studies based on astronomical observations of the local interstellar medium, on the other hand, suggested a much smaller upper limit of around 0.25 μm (silica) or 1 μm (graphite) for the size distribution of ISD particles. Therefore, it has been suggested that low-density fluffy dust particles may mimic the impact signals of heavier compact particles. In this work, we discuss a series of impact experiments that have been performed at the Heidelberg dust accelerator facility with the Cosmic Dust Analyzer flight spare unit, to compare the high-velocity impact ionization properties of compact and hollow silicate particles, and carbon aerogel particles with each other and with literature data. The experiments indicate differences in the collected total amount of impact charges and how quickly the charges are collected, between impacts from compact particles and their non-compact counterparts. The results of this first study suggest that fluffy particles generate less ions upon impact than their compact counterparts, opposite to the suggested explanation for the heavy ISD particles. Data from the performed impact experiments indicate that a secondary process (e.g. secondary impacts from ejecta or more target material ionization) could be the main cause for the observed differences. These results imply that the previously detected heavy ISD particles may be real. We identify the key problems with the performed dust experiments and advise that future impact ionization instruments should additionally be calibrated with improved low-density fluffy dust particles that better represent the properties of cosmic dust particles.

* Corresponding author.
E-mail address: silvan.hunziker@phys.ethz.ch (S. Hunziker).

https://doi.org/10.1016/j.pss.2022.105536
Received 23 March 2022; Received in revised form 23 June 2022; Accepted 1 July 2022
Available online 10 July 2022

1. Introduction

Cosmic dust detectors based on measuring the impact ionization charge of dust particles after high-velocity impacts on a target, have been flying in space since the early '70s. These provided a big leap forward in cosmic dust detection techniques owing to their multi-coincidence method for distinguishing dust impact signals from other noise sources (Grün et al., 2019). Such detectors were calibrated in the laboratory using an electrostatic dust accelerator, capable of accelerating conductive dust analogs to velocities of up to 80 km/s. Because dust analog materials have to be conductive in order to be accelerated, mostly compact "spheres" of Iron, Silicate or Carbon were used for calibrations in the laboratory (e.g. Goeller and Gruen, 1989; Stübig, 2002). Later, non-conductive materials with a conductive coating opened up the possibility to calibrate instruments using mineral samples (e.g. Fielding et al., 2015; Hillier et al., 2009). In 1993, the Ulysses Dust Detector System provided for the first time in situ measurements of interstellar dust (ISD) in the solar system (Grün et al., 1993).

The Ulysses data analysis revealed a solar-cycle dependence of the flux and flow direction for the submicron-sized particles (e.g. Landgraf et al., 2003; Strub et al., 2015; Sterken et al., 2015) due to the Lorentz force acting on the charged particles (Landgraf, 2000; Sterken et al., 2012). The Ulysses dust data also contained surprisingly heavy particles[1] of up to 10^{-13} – 10^{-12} kg (a few micrometer in radius) (Landgraf et al., 2000; Krüger et al., 2015). These were too heavy with respect to the constraints on the ISD mass distribution, which typically has an upper limit of 0.25 μm radius for silicates and 1 μm for graphite (e.g. Mathis et al., 1977; Weingartner and Draine, 2001; Draine, 2009). However, some more recent studies suggested that particles with sizes of several microns may exist in the ISM and from supernova dust (e.g. Wang et al., 2015; Gall et al., 2014; Gall and Hjorth, 2018, and references herein). The topic remains of discussion in the field.

Because of the discrepancy between in situ measurements of large ISD particles by Ulysses and the existing size boundaries from classical models, Sterken et al. (2015) suggested that impacts of low-density particles may perhaps mimic the impact signals of larger compact particles and the number of heavy ISD particles with masses of 10^{-12} kg may have been overestimated in the Ulysses data. This suggestion was based on:

1. *Impact ionization theory*: Elementary shock wave propagation physics suggests that a low density dust particle acquires more specific internal energy from the impact as compared to its compact counterpart of the same chemical composition. From this one might conclude that low density dust produces more ions during a high-velocity impact (Drapatz and Michel, 1974). Thus, low density dust particles of lower mass could mimic the impact ionization signal of high density dust with higher mass. The impact charge yield from a low density dust particle would have to be up to a few 100 times larger than the charge yield from a compact particle with the same mass and impact velocity to solve the discrepancy between in situ measurements and classical models.
2. *Indications of low-density dust from sample return and spacecraft data combined with simulations*: The Stardust ISD candidate samples that were brought back to the Earth, yielded micrometer-sized ISD particle candidates with surprisingly low densities (after capture) of less than 0.7 g/cm^3 (Westphal et al., 2014). Also combining spacecraft data and dust dynamics studies of ISD indicates that "large ISD grains" may be porous in nature (Sterken et al., 2015), while ISD smaller than about 0.2–0.3 μm seemed to be compact (Sterken et al., 2015; Altobelli et al., 2016). These studies have uncertainties though, e.g. selection effects in the Ulysses data or densities that may have been altered by the impact in the aerogel. Implications of porosity on measurements of interplanetary dust particles (IDP) can be significant as well, since IDPs are often found to be porous. Cometary dust investigated using an Atomic Force Microscope on-board of the Rosetta mission showed large (several microns) aggregate structures with smaller (100 nm) sub-components (Mannel et al., 2019). Other instruments on Rosetta yielded porous or fractal structures for larger (micron-sized) dust (Güttler et al., 2019). Furthermore, IDPs collected in the atmosphere are known to be porous in nature (Bradley and Brownlee, 1986; Rietmeijer, 1993; Love et al., 1994). Last but not least, also the plumes of Enceladus could be plumes of aggregate particles which — if unequivocally determined — does not rule out a vapor-based origin of the particles (Gao et al., 2016). In brief, low-density dust is ubiquitous in interplanetary, and likely also in interstellar space.
3. *Calibration of dust detectors is usually performed using compact dust analogs*: Appendix A gives a non-exhaustive overview of a number of relevant experiments and calibrations that have been performed with different dust and target materials in the past. No prior experiments have been performed to assess impact ionization for particles with identical composition but different structure or density.

Examining the effect of dust porosity on the impact ionization process can help to better constrain the upper size limit of the ISD size distribution from in situ measurements, which is important for understanding the processes of formation and destruction of ISD in the interstellar medium and for determining the gas-to-dust mass ratio in our local interstellar environment. It is also important for the interpretation of interplanetary – and in particular the cometary dust – from impact ionization data. Last but not least, this work represents a learning process of developing, coating, and accelerating new dust analogs and the experiments allow us to gain further insights in the impact ionization process. In brief, this work may have implications for three sub-fields of cosmic dust research: ISD, IDP, impact ionization.

Section 2 briefly describes impact ionization theory. Section 3 presents the experimental setup with a description of the dust analogs, the coating process, setup of instruments along the beamline, and target. Section 4 shows the results of the experiments: from mass distributions of accelerated dust particles, to impact charge yield after impact on the target and the rise time of the charge yield signal. Section 5 reviews and discusses these results after which conclusions are drawn and recommendations for future experiments are presented in Section 6.

2. Impact ionization theory

The first thing that happens when a dust particle hits a solid target is the generation of two shock waves: One moving backward into the dust particle and one propagating into the target in an approximately hemispherical shape, decreasing in strength with increasing distance from the impact location (e.g. Zel'dovich & Raizer, 1967). For low impact velocities these shocks may be weak, not more than an acoustic disturbance, but their propagation speed is never smaller than the velocity of sound (several km/s typically), which means that there is a first rapid ionization process (for small micron sized dust the shock travel time across the dust is on the order of nanoseconds). The main dissipative processes happen in these shocks, all following processes that are essentially isentropic. The partition of how much of the dissipated impact energy goes into the dust and how much into the target is determined by this initial shock dynamics and depends on the density ratio between dust and target. Low density dust is heated by a larger amount than its compact counterpart. In the present examples the dust is well above the vaporization limit, which means that the ionization process most probably happens within the bulk of the dust material, which is why this often is referred to as "volume ionization". Within this initial fast scenario a further ionization process has been discussed, denoted as "surface ionization" (Kissel and Krueger, 1987). It is connected to the exit of shock waves at free surfaces, either at

[1] Inferring the mass of the dust particle depends on a velocity determination, or alternatively on theoretical assumptions, which may have large uncertainties (Janisch, 2021).

the impacting dust or at the target. However, the details of this process are not well understood yet. For a more detailed description of the shock processes and an overview of the existing literature (see e.g. Mocker et al., 2013).

Apart from these fast occurring ions (often referred to as "primary ions") the measured ionization signal contains a second, slower contribution ("secondary ions") which is thought to originate from the target. This has been attributed to secondary impacts of target ejecta with surrounding structures (Ratcliff et al., 1997; Auer, 2001), but it is presently under discussion whether processes at the target itself better explain these secondaries. However, no matter what the detailed processes are, it can be expected that they increase with increasing target shock strength, which in turn means that they will be weaker for low density dust as compared to the case of compact dust.

The effect of reduced density therefore is expected to consist of an increase of dust ions but also in a decrease of target ions and a prediction of the net effect is difficult from theoretical arguments. That is why dedicated measurements are needed.

3. Experiments

3.1. Dust analogs: overview and suitability for acceleration

In order to compare impacts of compact with porous particles, analogs for porous particles were created in similar mass ranges and with as much as possible the same composition as their compact counterparts. Silicates and carbonaceous materials were used because they are major constituents of interstellar dust. Multiple different sizes of the compact particles were produced (see Section 3.2 and Table 1). "Batch I" mainly consists of bigger compact silicates (0.5–1.2 μm), while "Batch II" mainly consists smaller compact silicates (≈ 0.3 μm), similar to the sizes of the hollow silicates. Hollow silicate particles were created as a first approximation of an analog to porous particles (Fig. 1). The compact and hollow silicate particles were manufactured (Section 3.2) and then coated with a conductive polymer layer (Appendix B), so that they could be accelerated in the dust accelerator. Attempts were also made to coat and fly silicate aerogel as a better porous dust analog than hollow spheres, but although the aerogels were successfully coated, they were not successfully flown. Carbon aerogel dust particles (Fig. 2) were used for comparison with older measurements of compact carbonaceous materials from Stübig (2002). These particles did not need a conductive coating as they were conductive by themselves. The carbon aerogel flew well in the accelerator, but clumped very soon on the needle of the accelerator source (Fig. 3), causing them to stop flying altogether. Thus, only a small sample of impacts with carbon aerogels were obtained. The resulting size distribution of all the particles that were accelerated is discussed in Section 4.1 and Appendix D in order to learn which particles flew well and which ones were more difficult to accelerate. After characterization using microscopes and other devices (Laser particle size measurements, Energy Dispersive X-ray analysis, etc.), the dust particles were accelerated in a small test accelerator at the Max Planck Institute for Nuclear Physics prior to the full-scale experiments with the 1.8 MV van de Graaff dust accelerator. All particles were accelerated successfully in the test accelerator, except for the aforementioned Silicate aerogels. The Carbon aerogels were also tested at the small test facility at the Laboratory for Atmospheric and Space Physics at the University of Colorado, Boulder where similar issues occurred concerning clumping of particles on the accelerator source needle.

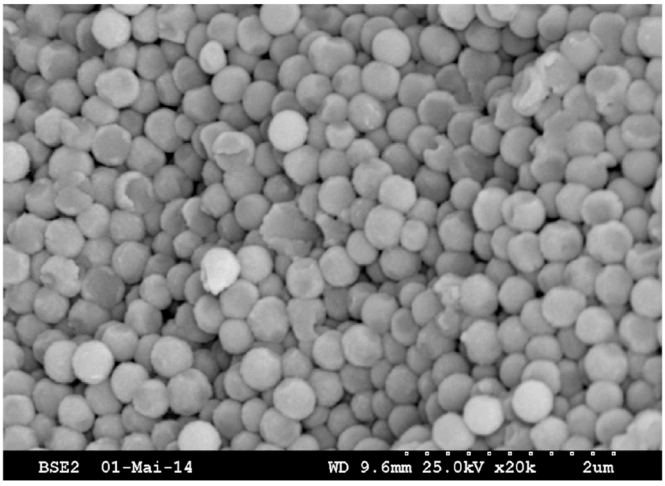

Fig. 1. Scanning Electron Microscope (SEM) image of the hollow silicate spheres, broken for the purpose of the imaging. These are the spheres before coating.

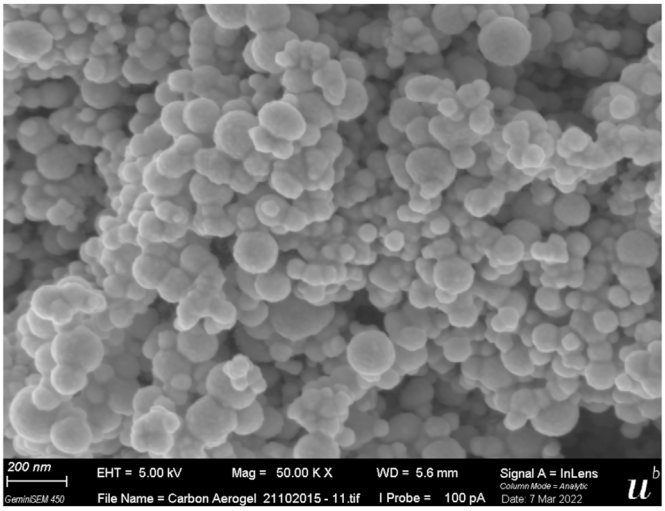

Fig. 2. SEM image of the carbon aerogel particles.

Table 1
Dust analogs used in the experiments. PPy is the polypyrrhole used for the coating (Section B). The compact carbon reference material was not flown in this study but taken from literature (Stübig, 2002). The material density is the density before coating. The size ranges quoted in the table correspond to the full range of particles that have been accelerated and seen by the detectors at the Particle Selection Unit.

Material	Function	Size (μm)	Density[1] (g/cm^3)	Coating	Accelerated	CDA Target
Compact silicate (Batch I)	reference material	0.05–6	2	PPy	yes	IIT + TOF
Compact silicate (Batch II)	reference material	0.06–5	1.96	PPy	yes	IIT + TOF
Hollow silicate	porous analog Si I	0.1–13	1.33	PPy	yes	IIT + TOF
Silicate aerogel	porous analog Si II	–	0.12–0.15	PPy	no	–
Compact carbon Stübig	reference material	1.2–3.2	2.2	–	Stübig (2002)	IIT + TOF
Carbon aerogel	porous analog C	0.2–10	0.2	–	Yes[2]	IIT

[1] Average particle bulk density measured with helium pycnometry.
[2] Material started to stick to the dust source needle and because of that could only be successfully accelerated for a short time.

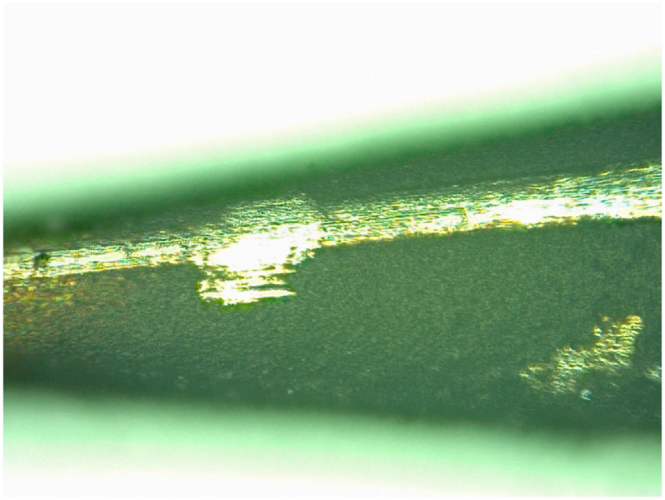

Fig. 3. The dust source needle, where carbon aerogel piled up and prevented further acceleration of carbon aerogel particles.

3.2. Dust analog production process

The compact silicates were manufactured using Stöber synthesis from TEOS (tetraethyl orthosilicate) in ethanol/water/ammonium hydroxide, functionalized using 3-(trimethoxysilyl)propyl methacrylate (MPS), and oxidised using ammonium persulfate, resulting in the production of monodisperse, compact silicate particles. For Batch II (the smaller compact silicates) the predicted mean particle diameter was 205 nm and the measured diameters were in the range 300–350 nm. The silicates were subsequently coated with polypyrrole (PPy), and the PPy coating process is described in Appendix B.

The hollow silicates were prepared using a two-step method based on the sol–gel process (Hah et al., 2003). The particles were manufactured from PTMS (phenyltrimethoxysilane), partially hydrolysed using nitric acid, then functionalized and coated with PPy as above, resulting in the production of monodisperse hollow silicate particles. The predicted mean particle diameter was 203 nm and the measured diameters were in the range 250–380 nm.

Silica aerogel powder was purchased from a commercial provider and surface characteristics (hydrophilic versus hydrophobic) were altered for further characterization (e.g. size distribution) and for the coating process using an oven. Carbon aerogel was ground from a monolith and subsequently filtered through a nylon filter for obtaining sufficiently small particle sizes.

The dust analogs were characterized before and after the coating process using different laboratory measurement devices. Field Emission Scanning Electron Microscope (FESEM) imaging was used for imaging the particle morphology after coating. Figs. 4 and 5 show FESEM images of the coated compact and hollow silicates used for these experiments.

3.3. Experimental setup and data extraction

The experimental setup along the accelerator beamline can be divided into a few main parts (see Fig. 6): the dust source, the section of the accelerator where dust is electrostatically accelerated, the Particle Selection Unit (PSU), several measurement devices along the beamline (at the PSU and one before the vacuum chamber, referred to as the Q_d-detector), and the cosmic dust analyzer (CDA).

3.3.1. Dust accelerator

The dust accelerator electrically charges and accelerates dust particles with a maximum voltage of 2 MV up to velocities of about 80 km/s (Mocker et al., 2011). The velocity v of an accelerated dust particle depends on its acquired surface charge q, mass m and the acceleration voltage U as shown in Eq. (1). The dust experiments described in this work were performed with voltages between 1.7 and 1.8 MV.

$$qU = \frac{1}{2}mv^2 \tag{1}$$

3.3.2. Particle Selection Unit

The Particle Selection Unit receives the information about the charge and velocity of the accelerated dust particles acquired by a chain of detectors at the PSU, and uses it to sort out particles with parameters outside of an user-defined surface charge, velocity and mass range. It also provides the time when the particles passed the instrument. This information, as well as the impact time registered by the dust analyzer, is used to determine the dust particle mass and velocity for each impact.

3.3.3. Q_d detector

Dust particles that passed the PSU selection, travel through a vacuum tube and pass the Q_d detector, which is mounted just before the dust analyzer. Like the PSU, the Q_d detector measures dust particle surface charge and velocity using and induction tube. This measurement serves as an independent source of information for the mass and velocity of the dust particles. Details about the process of matching the dust particle masses and velocities determined by the detectors at the PSU and the Q_d detector with the right CDA impact are discussed in Appendix C.

3.3.4. Cosmic dust analyzer (CDA)

The last part of the setup consists of a vacuum chamber which contains the CDA flight spare unit (Fig. 7). For details about the CDA, we refer to Srama et al. (2004) and Kempf et al. (2012). Dust particles that successfully passed the Q_d detector pass through the entrance grid (QP

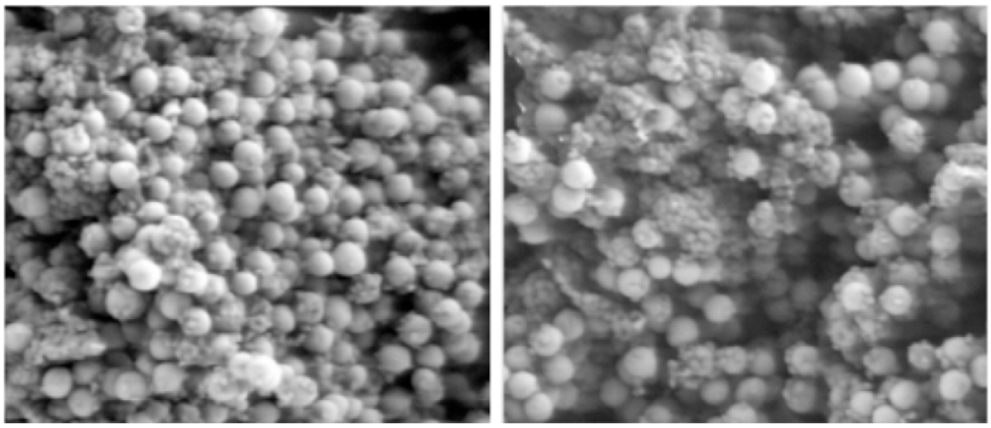

Fig. 4. Field Emission SEM images of the coated compact silicate spheres.

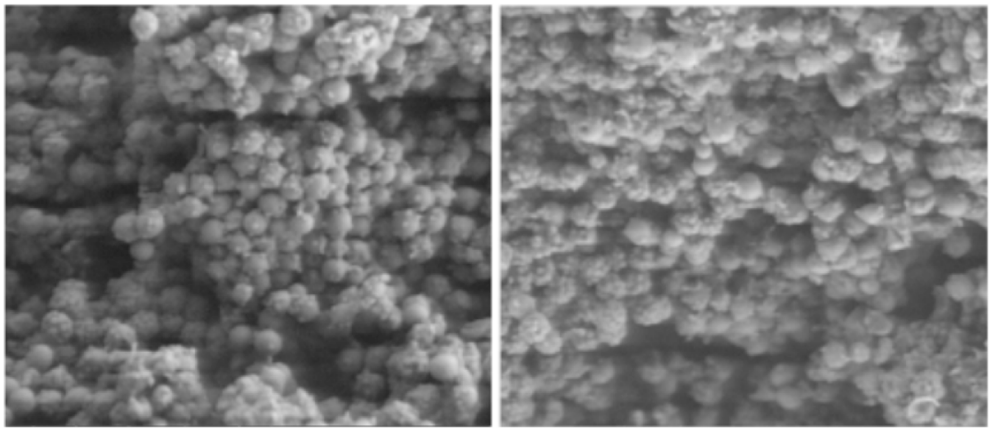

Fig. 5. FESEM images of the coated hollow silicate spheres.

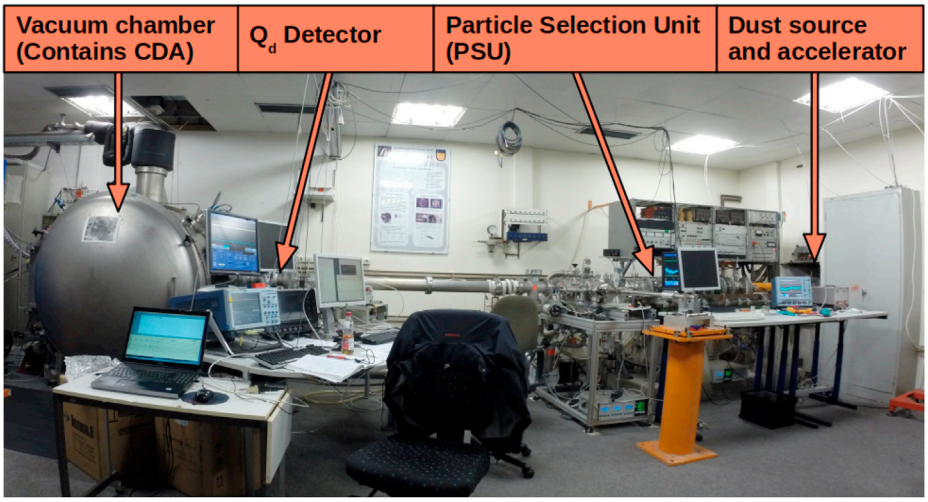

Fig. 6. The experiment setup in the laboratory with all five main components of the setup highlighted.

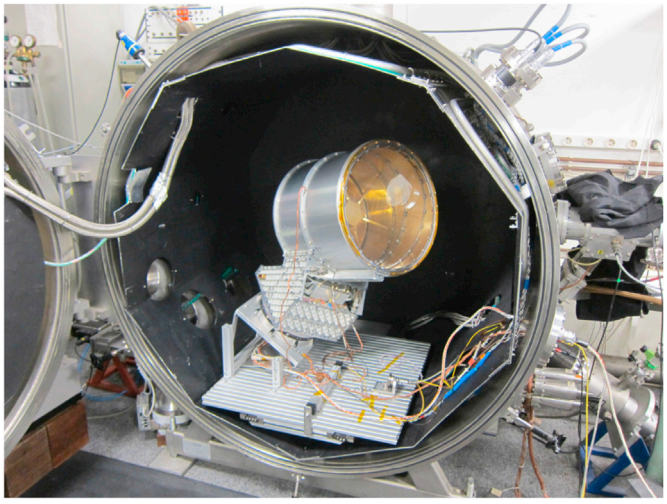

Fig. 7. The Cassini Cosmic Dust Analyzer flight spare instrument in the vacuum chamber of the accelerator in Heidelberg.

detector) in front of the CDA before hitting either the large, gold plated Impact Ionization Target (IIT) or the smaller rhodium Chemical Analyzer Target (CAT), depending on how the instrument was oriented in the vacuum chamber. Fig. 8 shows a schematic side view of the CDA with indicated locations of its major sub-instruments.

The QP detector is an integral part of the instrument and consists of several (shielded) grids at the entrance of CDA, which is capable of detecting the signal induced by charged particles that pass through the grids. Fig. 9 shows a typical QP signal of a fast (≈20 km/s) dust particle with a charge of about 25 fC. The time of the impact is marked by $t = 0$ s and the primary (pre-impact) QP signal of the entering particle is located at $t < 0$ s. The amplitude and the duration of the primary QP signal can be used to estimate the particle charge and velocity, respectively (Auer et al., 2002), but the results are less reliable than the measurements from the Q_d detector or the PSU because of the lower sensitivity and time resolution of the QP detector. The charge detection limit of the QP detector is ≈ 1 fC. The outgoing (post-impact) QP signal at $t > 0$ s is caused by charged particles (e.g. fragments or ions) which were created by the impact and exit CDA through the entry grid. Outgoing QP signals were only observed for fast impacts ($\gtrapprox$15 km/s) and often show an initial small peak followed by a larger secondary peak.

After a dust impact on either one of the targets, the negative impact charges are collected directly at the target (QT signal) and the positive charges are accelerated towards and collected at the ion grid (QI signal). Fig. 10 shows one example for the charge collection at both detectors after a high velocity impact on the IIT. The curves of the accumulated QT and QI charges reach a maximum roughly when all charges are collected but simultaneously discharge slowly with a fixed time constant (Srama, 2009). For our following data analysis, we extracted the QT and QI signal

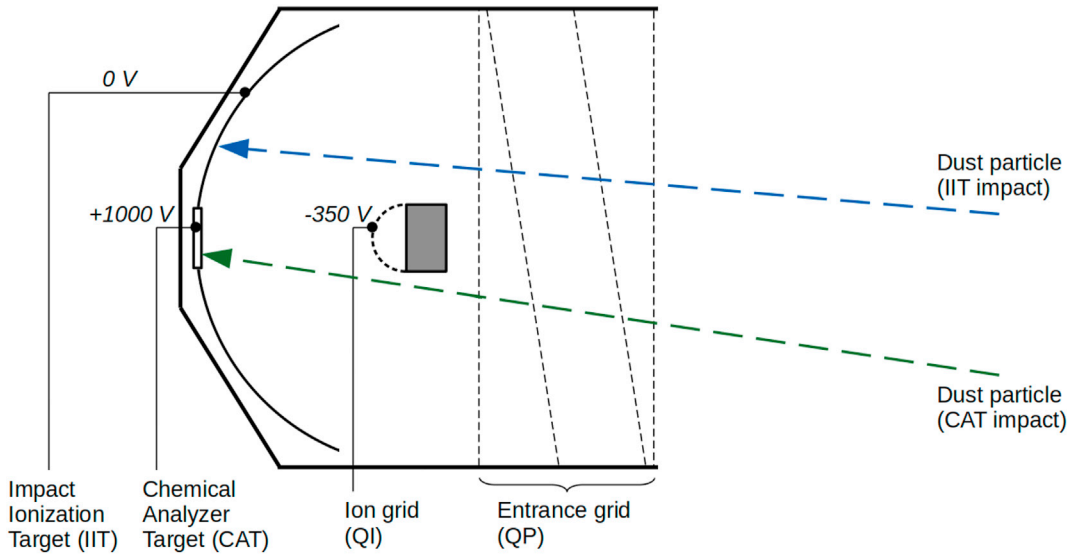

Fig. 8. Schematic cross section of the CDA instrument. The two arrows indicate possible trajectories of dust particles that impact on the large spherical IIT or the small central CAT. Negative charges from the impact plasma are collected directly by the targets. Positive charges are collected at the ion grid after being accelerated towards it by the electric field caused by the potential differences indicated in the schematic.

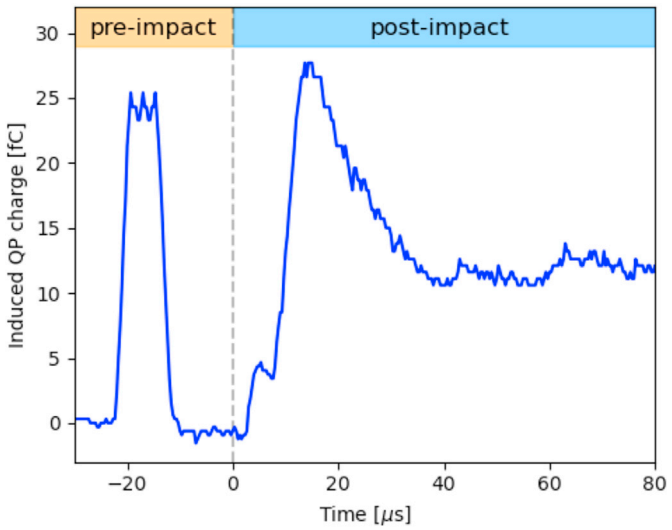

Fig. 9. Induced signal of a charged dust particle (hollow silicate) passing through the QP detector of the CDA. The impact time at $t = 0$ s is indicated by the vertical dashed line.

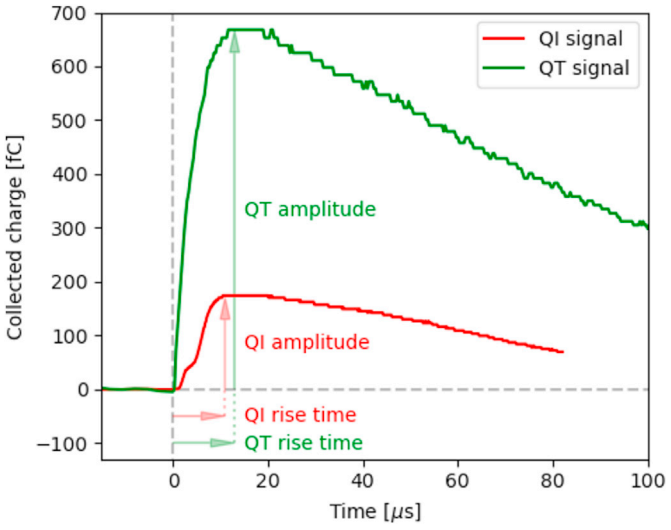

Fig. 10. QT and QI signals showing the negative and positive charges, respectively, which where collected at the detectors in the CDA over a few microseconds after a high velocity impact of a hollow silicate. A number of important measured properties - signal amplitudes and rise times - are schematically indicated by arrows.

amplitudes and rise times.[2] The signal amplitudes depend on the mass and velocity of the impacting dust particle, while the rise times were found to most likely depend on the impact velocity alone (Dietzel et al., 1973; Goeller and Gruen, 1989). The increasing slope of the QI signal is often divided into an initial steep slope that indicates the collection of the primary charges, followed by a less steep slope that indicates the collection of secondary charges (e.g. Ratcliff et al., 1996).

Dust impacts on the CAT would additionally allow to perform time-of-flight mass spectrometry on the positive impact charges. However, we have only been able to acquire about 30 good CAT mass spectra with H, C, Si and Rh lines from the "Batch II" compact silicates. The Rhodium lines are from material of the Rhodium target. This was not enough for a comprehensive study but it aided with the analysis of some crucial particle properties (see Section 4.1, Compact silicates from Batch II).

4. Experimental results

4.1. Mass distributions of accelerated dust

Fig. 11 shows the mass distributions of the dust particles that were measured by the different detectors for each dust sample. The distributions in green are the closest representation for the particle masses that were present in the individual dust samples because they show the collection of all dust particles that exited the dust source and accelerator, and were measured by the detectors at the PSU. The distributions in red show which of the accelerated dust particles were allowed to pass through the PSU.[3] Panels (a) and (c) also show the estimated mass range

[2] The time difference between 10% and 90% of the signal amplitude.

[3] PSU selection was changed throughout the measurements for operational reasons.

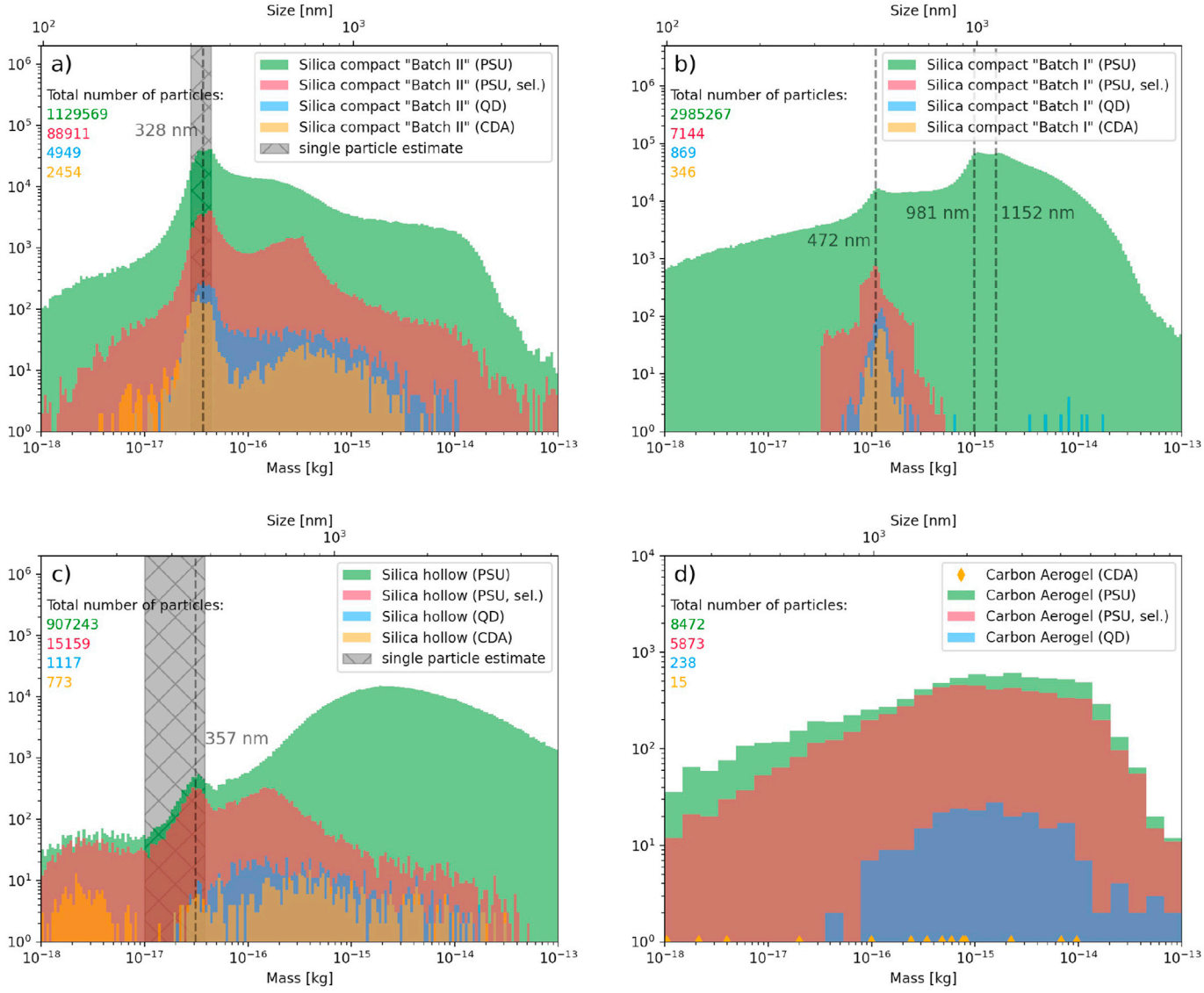

Fig. 11. (a) The mass distributions for the dust particles that were registered by the detectors at the PSU (green), allowed to pass through the PSU (red), detected by the Q_d detector (blue), and produced identifiable impacts on CDA (orange) for the compact silicates from Batch II. Panels (b), (c) and (d) show the corresponding distributions for the compact silicates from Batch I, the hollow silicates and the carbon aerogel dust particles, respectively. The individual CDA impacts for carbon aerogel are marked as diamonds on the bottom of panel (d) because the total number was very small. The total number of particles measured by the individual instruments are listed on the top left for each dust type.

for the single compact and hollow silicate dust particles (shaded areas). Both samples are supposed to be mono-disperse. The mass ranges were estimated based on particle size measurements with FESEM (see Section 3.2) and the average particle bulk density measured with Helium pycnometry (see Table 1). The additional weight of the PPy coating is not included in this estimate but it only adds about 20–30% additional mass to the silicate dust particles on average. The mass distributions help us better understand the structure of the particles that produced the observed impacts on the CDA. This is crucial because our aim is to identify differences in the impact ionization signals caused by a difference in the particle structure (e.g. particle density).

4.1.1. Compact silicates from Batch II

The location of the prominent peak inside the single particle mass estimate around $3.7 \cdot 10^{-17}$ kg in Fig. 11(a) indicates that the sample of compact silicates from Batch II is dominated by single dust particles with a diameter of about 330 nm (with measured average particle bulk density of 1.96 g/cm^3, from Table 1). Therefore, the shape of the distribution suggests that – for the this sample of compact silicates – a vast majority of the CDA impacts (colored in orange in Fig. 11) with masses 10^{-17} – 10^{-16} kg must have been produced by single compact silicate particles. The broader maximum for the CDA impacts of masses $> 10^{-16}$ kg is likely the result of impacts from clusters of multiple compact silicates that stuck together. The full mass-velocity distribution for the compact silicates from Batch II is shown in Fig. 17(a) in Appendix D. The full distribution also shows the prominent mass peak for the single particles, and it additionally shows that some of the compact silicates exhibited significantly more surface charge than the average, and thus were able to reach velocities up to about 30 km/s. Some of the CDA impacts have exceptionally low masses ($< 10^{-17}$ kg), and therefore were likely caused by pieces of PPy coating. This is supported by our analysis of a small number of CAT impacts for this particular dust sample, which has found evidence for a lack of Silicon in the mass spectra of many such low mass impacts.

4.1.2. Compact silicates from Batch I

The bigger compact silicates from Batch I consisted of a mixed sample

with multiple different sizes, as indicated by the three highlighted mass peaks in the PSU mass distribution in Fig. 11(b), or the three highlighted particle sizes in Fig. 17(b). The peaks are located at masses of $1.1 \cdot 10^{-16}$ kg, $9.9 \cdot 10^{-16}$ kg and $1.6 \cdot 10^{-15}$ kg, which results in estimated particle diameters of 470 nm, 980 nm and 1150 nm, respectively (with measured average particle bulk density of 2 g/cm^3, from Table 1). For this dust sample, the PSU selection was adjusted such that only the smallest sizes of the compact silicates from Batch I would pass through. This narrow selection limited the total number of CDA impacts but it also ensured that most of the impacts were produced by single compact silicates instead of clusters of pieces of coating.

4.1.3. Hollow silicates

The mass peak around $3.1 \cdot 10^{-17}$ kg in Fig. 11(c) indicates that the single hollow silicates had a diameter of about 360 nm (with measured average particle bulk density of 1.33 g/cm^3, from Table 1). However, the distribution before the PSU selection shows that most of the hollow silicates must have been stuck together in massive clusters. As a consequence, the number of CDA impacts from single hollow silicates (10^{-17} – 10^{-16} kg) is relatively small compared to the number of impacts from clusters ($> 10^{-16}$ kg). Most of the heavy clusters were sorted out by the PSU because heavy particles are accelerated to lower velocities (see Eq. (1)), and the lowest velocity limit for the PSU was set to 3 km/s. It is unclear at this time why the hollow silicates would be more prone to clustering but it seems to be the reason for having a lot less CDA impacts from single hollow silicates. The CDA impacts of the hollow silicates also show a distinct peak at low masses $< 10^{-17}$ kg. Particles that small are most likely just pieces of PPy coating as well.

4.1.4. Carbon aerogel

Fig. 11(d) shows that most of the carbon aerogel dust particles were either relatively heavy or clustered as well. The mass distribution for the PSU selected particles is broad and peaks around 10^{-15} kg, which corresponds to a diameter of about 2 μm for the low density of the carbon aerogel (0.2 g/cm^3). Most of the few registered CDA impacts from carbon aerogel particles that could be identified had masses in the range 10^{-16} – 10^{-14} kg, but some of the fast ones were significantly smaller with masses $< 10^{-17}$ kg. The full velocity-mass distribution is also given in Fig. 17(d).

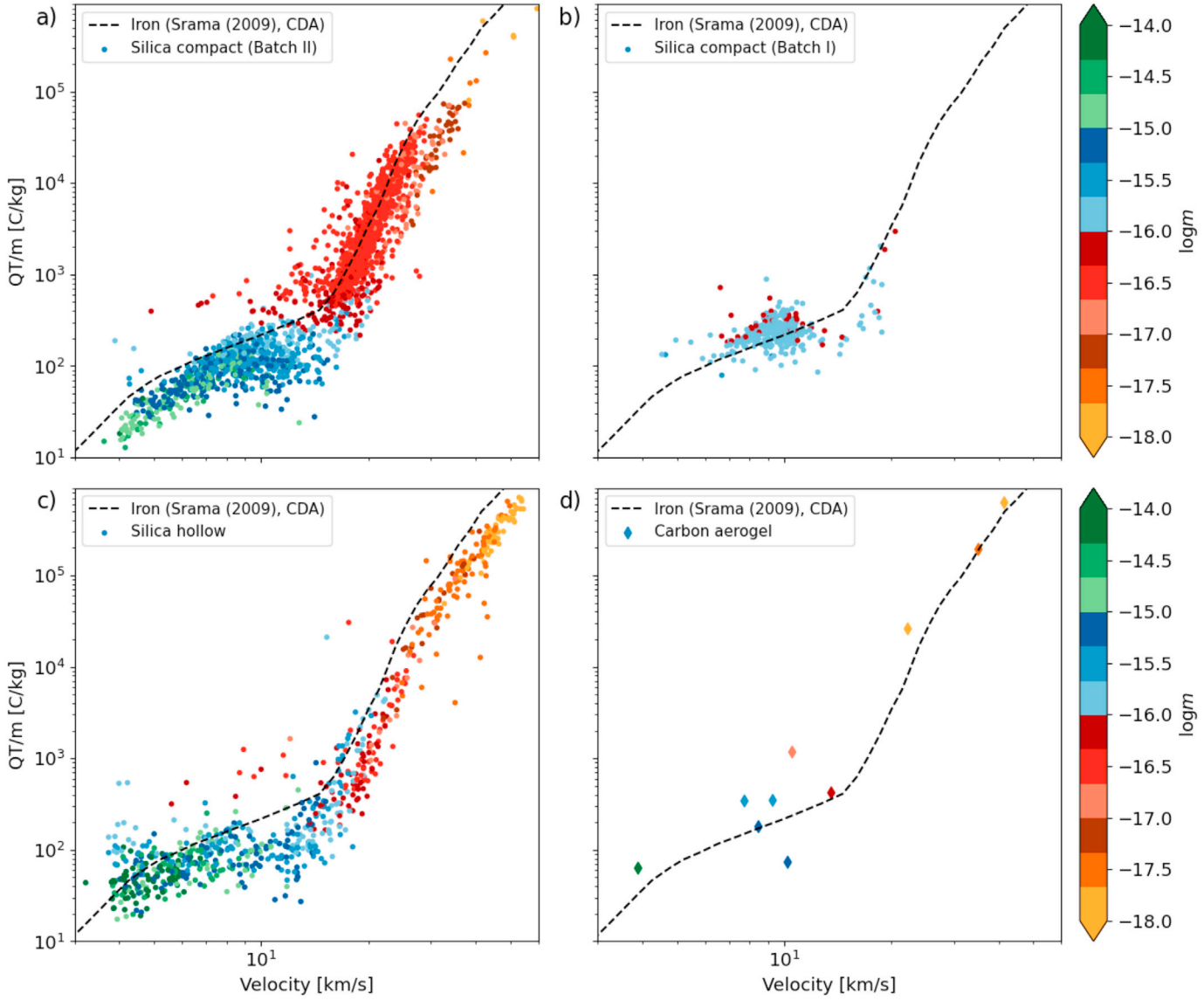

Fig. 12. (a) Negative charges measured on impact per unit projectile mass depending on the impact velocity for the compact silicates from Batch II, (b) the compact silicates from Batch I, (c) the hollow silicates and (d) carbon aerogel. Projectile masses are indicated with colors. As a common reference, all data are compared to literature values from Srama (2009) for iron particle impacts on CDA.

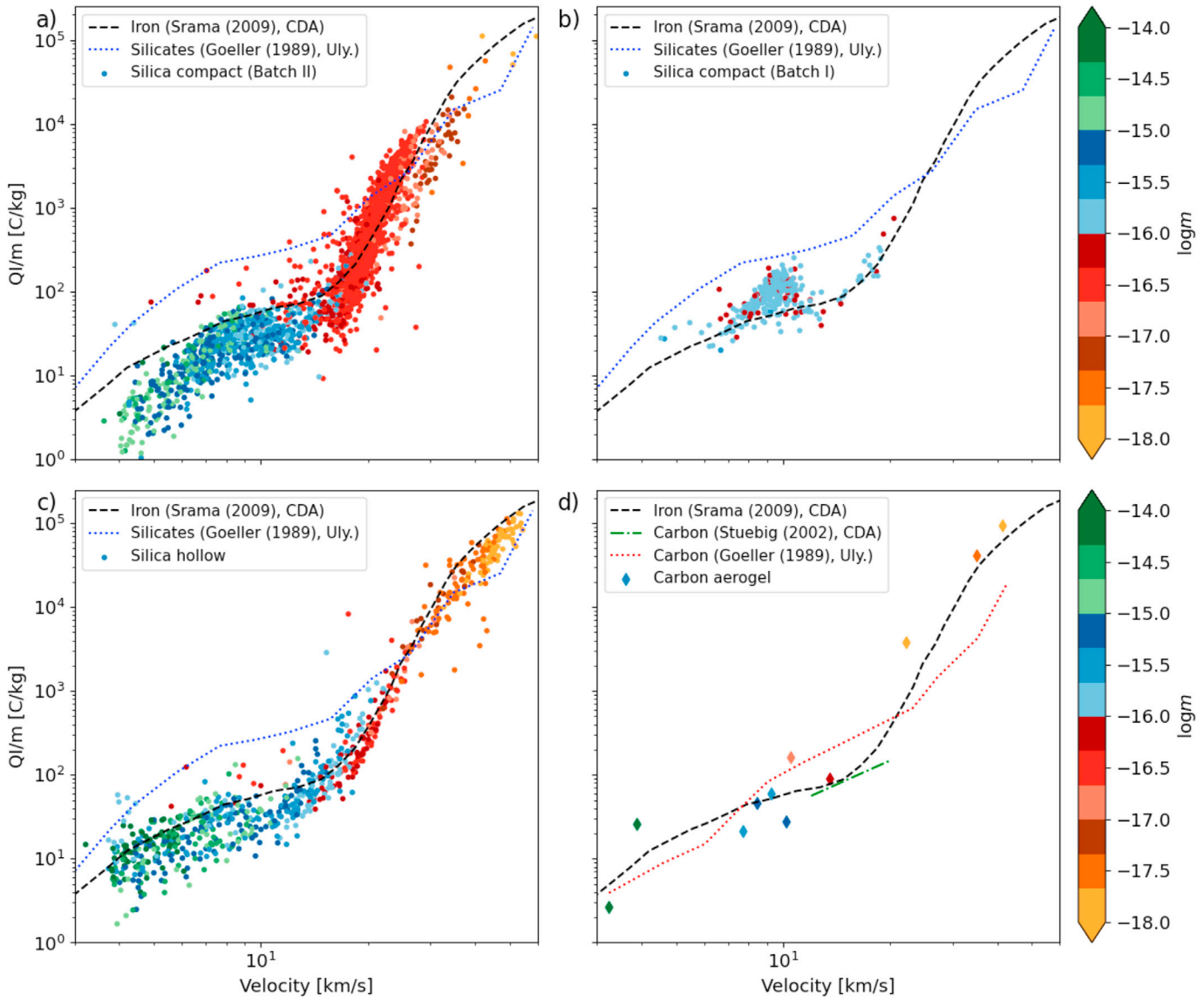

Fig. 13. (a) Positive charges measured on impact per unit projectile mass depending on the impact velocity for the compact silicates from Batch II, (b) the compact silicates from Batch I, (c) the hollow silicates and (d) carbon aerogel. Projectile masses are indicated with colors. As a common reference, all data are compared to literature values from Srama (2009) for iron particle impacts on CDA. The results for carbon aerogel are additionally compared to literature values from impacts of compact carbon particles on CDA reported by Stübig (2002). All results are also compared to the literature values from measurements of compact silicates and carbon with the Ulysses/Galileo dust detector reported by Goeller and Gruen (1989).

4.2. Impact charge yield

Fig. 12 and Fig. 13 show the negative charge amplitude (QT) measured at the IIT and the positive charge amplitude (QI) measured by the ion grid, respectively, per unit projectile mass for each dust sample. The results are compared to literature data from earlier CDA measurements with iron dust particles (Srama, 2009) as a common reference. Additional data from the literature is provided from CDA measurements of compact carbon particles by Stübig (2002), and Ulysses/Galileo dust detector measurements of QI/m for compact carbon and silicates[4] by Goeller and Gruen (1989). The Ulysses/Galileo dust detector is similar to the IIT, with a hemispherically shaped and gold plated target of similar size, and the same acceleration voltage (−350 V) for the impact charges. Therefore, the produced impact charges should be comparable. However, the results are not expected to be exactly the same due to differences in the measurement electronics and sensors.

The measured charge yield amplitudes QT and QI mainly depend on the projectile mass and velocity. An additional dependency on the ratio of projectile and target bulk material density has been theoretically derived in Drapatz and Michel (1974). Weak dependencies on the particle composition and the direction of the impact with respect to instrument orientation have been investigated and confirmed by (Goeller and Gruen, 1989). In this section, we will focus on highlighting differences between the charge yield measurements that may be caused solely by different particle structures or densities.

4.2.1. Mass and velocity dependence of the charge yield

In this subsection, we investigate the mass and velocity dependence of the charge yield for the compact silicates from Batch II and the hollow silicates. For the other dust samples there is not enough data to perform a reliable analysis. The charge yield as a function of impact velocity v and mass m is usually parameterized with the empirical equation:

$$Q = K \cdot m^{\alpha} \cdot v^{\beta} \tag{2}$$

[4] QT/m is not provided by the authors.

Table 2
Velocity exponent that describes the charge yield QT and QI with Eq. (2) with $\alpha = 1$ for compact and hollow silicates in the fast and slow impact velocity regimes.

Compact Silicates (Batch II):	β_{QT}	β_{QI}
slow (4 km/s $< v <$ 10 km/s)	2.1 ± 0.1	3.0 ± 0.1
fast (20 km/s $< v <$ 50 km/s)	5.4 ± 0.2	5.8 ± 0.2
Hollow Silicates:	β_{QT}	β_{QI}
slow (4 km/s $< v <$ 10 km/s)	1.0 ± 0.1	1.6 ± 0.1
fast (20 km/s $< v <$ 50 km/s)	6.4 ± 0.1	5.8 ± 0.1

Fig. 12 and 13 show that the velocity dependence significantly changes around 15 km/s. This is likely caused by the transition from the surface ionization regime at low impact velocities into the volume ionization regime at high impact velocities. Equation (2) thus has to be applied separately to the low velocity and high velocity regimes. Previous experimental studies have found $\alpha \approx 1$ (e.g. Dietzel et al., 1973; Goeller et al., 1986; Goeller and Gruen, 1989) for different particle compositions and instruments in both velocity regimes. The dependence on the velocity was found to be much stronger with $\beta \approx 1.2$–6.5 (e.g. Auer, 1994; Stübig, 2002; Mocker et al., 2013), depending on the projectile and target material, and on the impact velocity regime.

It is not possible to determine both power-law indices α and β independently because particle mass and velocity are intrinsically correlated in our data because of the linear electrostatic accelerator (see Appendix D and Eq. (1)). Therefore, we assume that $\alpha = 1$, as suggested by previous work, and that the specific charge yield QT/m and QI/m only depends on the impact velocity. This enables us to determine the velocity exponents β for compact and hollow silicates.

The resulting velocity exponents β for the measured charge yield QT and QI, which are summarized in Table 2, are consistent with the large range of values that can be found in the literature. For both dust types, the velocity dependence is strong with $\beta \approx 6$ for fast impact velocities. It has been suggested that the velocity exponent at fast velocities increases with increasing difference between the density of the projectile and target material (Drapatz and Michel, 1974; Hornung and Drapatz, 1981; Mocker et al., 2013). This would provide a good explanation for the large β-value, because of the large density difference between the silicate projectiles and the gold target. The velocity exponents β can get very small for slow impact velocities from hollow silicates, however, not unusually low compared to other data from the literature.

The velocity exponents β for compact and hollow silicates can differ by more than the reported uncertainty, but we argue that the differences between the two dust types are not large enough to be significant. This is because the reported 1-σ uncertainties only include the error from the fit of Eq. (2), but it does not include other sources of statistical bias: the amount of slow but heavy, and fast but light particles differ strongly in the datasets for the two dust types, and the spread in the charge released due to this may influence the slope of the fit. We believe that this kind of selection bias may explain some of the differences between the velocity exponents.

4.2.2. Comparison of charge yields for different compact silicates (Batch I and Batch II)

For the charge yield QT/m (Fig. 12) and QI/m (Fig. 13) we see a significant difference between the results for the smaller compact silicates from Batch II (a) and the bigger compact silicates from Batch I (b) at impact velocities around 10 km/s: the compact silicates from Batch I on average exhibit a larger charge yield at the same impact velocity. For impact velocities in the range 8–12 km/s and particle masses in the range $(1–2) \cdot 10^{-16}$ kg the median QT amplitude is about 1.2 times larger and the median QI amplitude is about 2.6 times larger. This is especially interesting because at this velocity – and respective particle mass – all compact silicates from Batch I should be single big compact particles, while the compact silicates from Batch II are likely to be clusters of multiple small compact silicates. This observation suggests that a single compact silicate particle has a larger charge yield than a cluster of smaller compact silicates of equal mass.

One could argue that the amount of PPy coating could affect the charge yield as well. An agglomerate of small dust particles should have a larger surface area than one big dust particle with the same mass, therefore the amount of coating material should be larger on the agglomerate. However, in all cases the PPy coating was added in percent dust particle weight, adding on average about 20% weight to the individual dust particles. As a consequence, the amount of coating on each single dust particle or agglomerate should only depend on its mass, and not its surface area.

4.2.3. Comparison of charge yields for compact (Batch II) and hollow silicates

Another possibly significant difference for the specific charge yield QT/m and QI/m can be seen between the compact silicates from Batch II (a), and the hollow silicates (c), in the velocity range 20–30 km/s and the mass range 10^{-17} – 10^{-16} kg (red). This parameter range is special because for both dust samples it belongs to impacts from single particles (as opposed to particle fragments or particle clusters). Especially the QT/m plots indicate visually that the single compact silicates on average may have a larger charge yield than the single hollow silicates at the same impact velocity. We see no order of magnitude difference with these particles (which is no surprise since, we have only 30% difference in density between the two dust types) and it is hard to compare impacts with exactly the same mass. Therefore, we will provide a closer investigation of individual QT and QI signals with equal masses and impact velocities between 23–26 km/s, where we have sufficient data to do so (see Section 5.3).

One could argue again that some of the difference is due to the PPy coating. The hollow silicates are larger at the same mass, and therefore can take more coating material per particle. However, the average mass of PPy coating per particle is less than 10% larger for the hollow silicates than for the compact particles (see Appendix B) . In addition, the density of PPy and the ionization potentials of its constituents are similar to SiO_2. Hence, we would not expect this to be able to explain a difference of a factor of two in charge yield.

At the high velocity end (> 30 km/s) both compact and hollow silicates have an equal charge yield, however, we argue that most particles at such high velocities and low masses ($< 10^{-17}$ kg) are likely to be pieces of PPy coating in both samples and therefore should not produce a different signal. At the low velocity end (< 6 km/s), the results seem to deviate as well, but this is hard to verify because there are many more heavy and slow particle clusters in the hollow silicate data. This abundance of heavy clusters in the hollow silicate data could bias the charge yield towards larger values.

4.2.4. Charge yield for carbon aerogel

The specific charge yield QI/m for the carbon aerogel particles shown in Fig. 13(d) follows very closely the literature values for iron from (Srama, 2009) – and for velocities < 15 km/s – also the values for compact carbon (Stübig, 2002). The QT/m measurements in Fig. 12(d) also follow closely the literature values for iron particles. These findings will be discussed further in Section 5.4. Due to the small amount of available data for carbon aerogel and the limited amount of compact carbon data with CDA (only from the literature), we are currently unable to identify significant differences between any compact carbon data and our measurements from carbon aerogel impacts.

4.3. Charge signal rise time

Figs. 14 and 15 show the measurements of the charge signal rise time for the negative charges QT and positive charges QI depending on the impact velocity, respectively, for each dust sample. The results are compared to the CDA calibration curves provided in Kempf et al. (2012)

for measurements with iron particles, because there are no other comparable data available. The data show a few differences to the literature values and between our dust samples, which will be highlighted in this section.

4.3.1. Rise time discontinuity around 20 km/s

At impact velocities > 20 km/s, we observe for the compact (a) and hollow silicates (c) a sudden drop of the signal rise time to values far below the calibration curves. This is a striking feature for which we have not found any reports so far. We find no direct connection between the discontinuity of the rise time and the transition from surface ionization to volume ionization because the transitions because the former happens at ~ 15 km/s and the latter at ~ 20 km/s. We also find no indication that the discontinuity is related to a significant change in particle properties. As shown in Figs. 14(a) and 15(a), the discontinuity of the rise time occurs for dust particles that belong to the single compact silicates from Batch II, all of which have similar masses in the range $(3.7 \pm 1.2) \cdot 10^{-17}$ kg, and are therefore expected to have a similar properties as well. The same discontinuity may also be partially visible in the rise time measurements for the compact silicates from Batch I (b) and the carbon aerogel (d), however, there is not enough data available to confirm it at this time. The discontinuity puts the data well below the calibration curve with iron particles.

This feature is strictly speaking not of large importance for the investigation of the difference in charge yield between compact and porous dust particles. However, we highlight it because we have not found any reports about this so far and it may result in a systematic overestimation of the impact velocities for CDA (or Ulysses) impacts above 20 km/s, in case the rise time would be used as an indicator for impact velocity (e.g., Fig. 5 (top) in Krüger et al., 2015).

4.3.2. Comparison of rise times of compact (Batch II) and hollow silicates

The rise times between the compact silicates from Batch II (a) and the hollow silicates (c) are mostly identical, which may also be due to the large spread of the data. However, the most significant difference can again be seen between the single compact silicates (a), and hollow silicates (c), in the mass range $10^{-17} - 10^{-16}$ kg (red). The QI rise time for compact silicates in the velocity range 20–30 km/s just after the discontinuity drops to values of about 9 µs, while for the hollow silicates the QI rise time drops to about 5 µs. This could be an indication for a

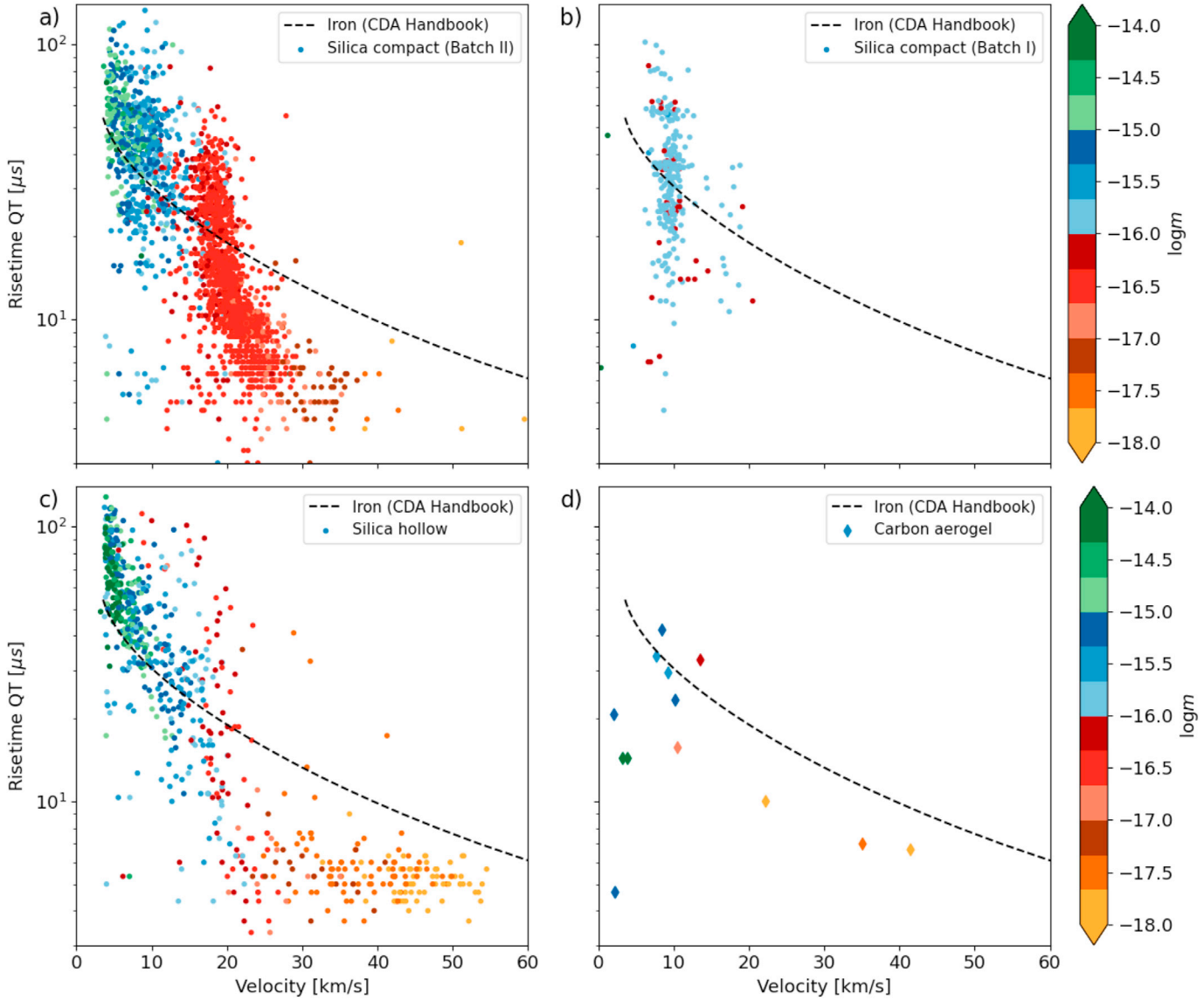

Fig. 14. (a) QT signal rise time depending on the impact velocity for the compact silicates from Batch II, (b) the compact silicates from Batch I, (c) the hollow silicates and (d) carbon aerogel. Projectile masses are indicated with colors. The data are compared to literature values from Kempf et al. (2012) for iron particles measured with CDA.

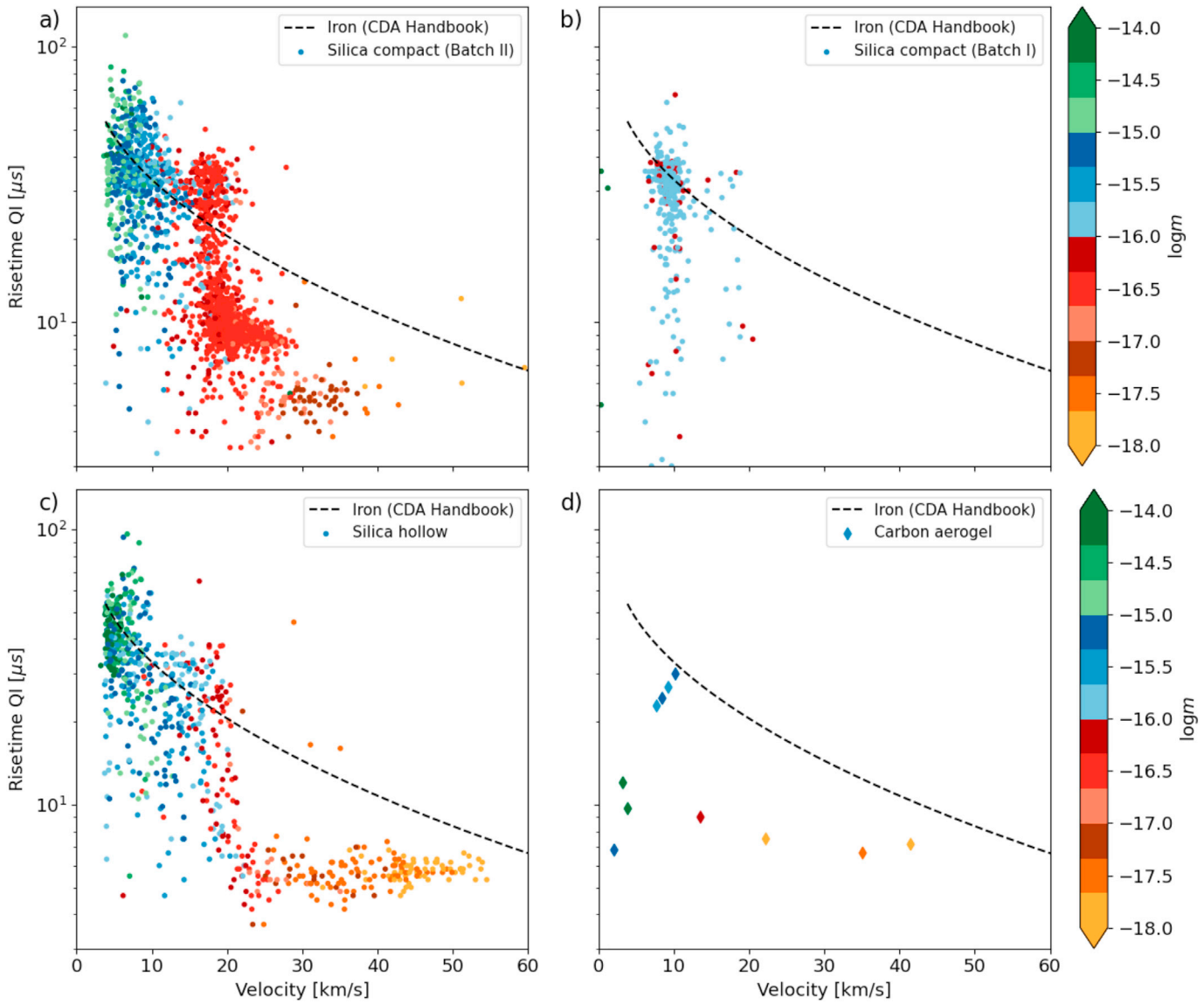

Fig. 15. (a) QI signal rise time depending on the impact velocity for the compact silicates from Batch II, (b) the compact silicates from Batch I, (c) the hollow silicates and (d) carbon aerogel. Projectile masses are indicated with colors. The data are compared to literature values from Kempf et al. (2012) for iron particles measured with CDA.

difference between the mechanisms of the impact ionization process for compact and hollow silicate particles.

4.3.3. *Rise times for carbon aerogel*

The rise times for carbon aerogel (d) are roughly consistent with the measurement for the other dust samples. The asymptotic rise time for large velocities of about 7 μs seems slightly larger compared to the compact silicates from Batch II (a) and hollow silicates (c). However, due to the small amount of available data and the lack of rise time data for compact carbon, it is not possible to make any firm statements about the effect of the low density at this time.

5. Discussion

The main results identified in the previous section can be summarized as follows:

- The rise time dependence on the impact velocity for compact and hollow silicates (and possibly carbon aerogel) is not strictly monotone and has a discontinuity around 20 km/s.
- Impacts from single compact silicates may produce more impact charge compared to clusters of smaller compact silicates with the same mass at impact velocities around 10 km/s.
- Impacts from single compact silicates may produce more impact charge with a longer QI signal rise time compared to hollow silicates with the same mass at impact velocities 20–30 km/s.
- Impacts from carbon aerogel seem to produce more or less as much specific charge compared to compact iron particles from the literature for various velocities (albeit based on a very small dataset for carbon aerogel impacts).

Possible reasons for the observed differences and implications for dust measurements will be discussed in this section. The consequences of these for ISD measurements are also discussed in Section 6.2.

5.1. *Rise time discontinuity at 20 km/s*

The precise calibration of the QI and QT signal rise times can sometimes be the only way to determine the impact velocity of a dust particle from measurements (e.g. the Ulysses dust detector). However, the rise

times in Section 4.3 show that this may be difficult for particle impacts at high velocities because of a discontinuity around 20 km/s, because we see no strictly monotone dependence anymore at higher velocities and the results at such high velocities differ significantly from the calibration curves provided in Kempf et al. (2012). The occurrence of a discontinuity in the rise time seems not to depend on particle properties (e.g. compact or hollow), but it may be important because of its possible implications for cosmic dust measurements nevertheless, it has not been reported in detail before, and it may facilitate to further advance our understanding of the physics of impact ionization in follow-up studies.

The deviations that we found show that impact velocities could be overestimated by the calibration curves by up to a factor of 3 in the most extreme cases. For example, based on the signal rise time, an impact with a velocity of 20 km/s could falsely be interpreted as an impact with a velocity of 60 km/s. As a consequence, the expected specific charge yield QT/m and QI/m would be overestimated by a factor of up to 1000, depending on the power-law index β (e.g. $3^6 = 729$). This could lead to an underestimation of the particle mass by orders of magnitude at such high velocities.

Although the rise time discontinuity seems not to depend on the structure or composition of the particles, it could significantly shift the mass distribution of the detected ISD. The results would indicate that some of the ISD impacts may be produced by much heavier dust particles than previously derived using the signal rise time. Therefore, it cannot definitely serve as an explanation for the unexpectedly heavy ISD particles mentioned in Section 1. Due to the large uncertainties, the signal rise time is usually not used exclusively to determine the dust impact velocity, thus implications on previous measurements with CDA (and possibly the Ulysses dust detector as well) should be small. However, it is still important to be aware of this discrepancy.

5.2. Charge yield from compact particles vs. particle clusters

This study did initially not intend to use silicate particle clusters as a fluffy dust analog for compact silicates, but the results have serendipitously revealed an interesting trend. Figs. 12 and 13 indicate that the charge yield per mass for silicates that supposedly consist of an agglomerate (or cluster) of compact particles is lower compared to a single big compact silicate of equal mass. At this time, we do not fully understand the cause of the different charge yield, and a full theoretical analysis is out of the scope for this paper. However, if the observed trend can be confirmed by other experiments and we interpret the particle clusters as fluffy dust analogs, we conclude that the fluffy dust analog in this case produces less impact ions at the same impact velocity than its compact analog of equal mass. This could result in an overestimation of the impact charge yield of a potentially fluffy dust particle by about a factor of 2, and therefore an underestimation of its mass by the same factor. This result would contradict the hypothesis for this study, which states that fluffy dust particles would have to produce more impact charge to be able to explain the unexpectedly heavy ISD particles (see Section 1).

However, this particular comparison between impacts of compact particles and particle clusters of equal mass was only possible in the velocity range 8–12 km/s. This is much lower than the usual impact velocities of ISD particles of more than 20 km/s. This leaves open the question as to whether the difference also exists for higher velocity impacts of particle clusters. Especially also because the impact ionization regime may be different (volume ionization instead of surface ionization) at larger velocities.

5.3. Signal shapes from compact particles vs. hollow particles

Most of the single compact silicates from Batch II and the hollow silicates had masses between $10^{-17} - 10^{-16}$ kg and therefore similar velocities in the range 20–30 km/s. Thus, there are plenty of impacts from both dust types in this particular parameter range, that allow a more statistically significant comparison of the signal shapes, and a further investigation of the cause of the observed differences seen in Section 4. Coincidentally, this velocity range is especially relevant for ISD impacts because it corresponds to the typical impact velocities for ISD particles with respect to Ulysses.

Fig. 16 directly compares the median QT, QI and QP signals of a number of impacts from single compact and hollow silicates with similar velocities and masses inside the mentioned parameter range. The spread of the data is relatively large, but it clearly shows the previously noted differences between the QI and QT signal amplitudes and rise times. The average measured QT and QI amplitudes are larger by about a factor of 2 for the compact silicates and it takes a significantly longer time for the QI signal to rise to the maximum, resulting in longer QI rise times for the impacts of compact silicates.

The QI signals shown in Fig. 16 consist of a fast rising primary component directly after the impact and a subsequent slow rising secondary component. Some authors suggest that this is because the impact ionization process consists of multiple stages (Ratcliff et al., 1996, 1997; Stübig, 2002; Srama, 2009): The primary impact produces impact charges as well as additional ejecta particles. The primary impact charges are collected by the detectors within a few μs after the impact, while the ejecta cause secondary impacts on the target and the surrounding structures. These secondary impacts produce additional delayed charges that are subsequently collected by the detectors as well. The secondary charges further increase the QT and QI signal amplitudes and rise times (Ratcliff et al., 1996; Srama, 2009). Therefore, the total charge yield depends on the number of produced primary charges and the number, velocity and trajectory of ejecta particles. However, the mechanism that causes the slow rising secondary component is highly debated in the community. Other mechanisms could be important as well, for example the amount of ionized target material depending on the particle structure.

The shapes of the QI signals in Fig. 16 reveal that both the increased amplitude as well as the longer rise time for the compact silicates are mainly due to the longer slow rising secondary component. Based on the analysis presented in Ratcliff et al. (1996), this may suggest that the difference between the signals from compact and hollow silicates could be caused by a different distribution and/or amount of impact ejecta, resulting in a smaller amount of secondary impacts for the hollow silicates. The authors theorized that the “fluffyness” of an impactor could influence the number and distribution of ejecta particles. Alternatively, we speculate it can be caused by more ionized target material for compact particles. Heavy ions from the gold target would take a longer time to reach the ion detector, and could therefore also explain the longer signal rise time.

The outgoing QP signals (i.e. QP signals after the particle impact) in Fig. 16 also exhibit a much larger peak for the compact silicates. This observation suggests as well that there may be a larger amount of charged material from secondary impacts or target material that leaves CDA after an impact from a compact silicate. The QP signals in Appendix E show a similar trend for the fast velocities (> 15 km/s). However, the impact ionization process is complex and it is currently unclear if any other mechanisms could have a similar effect on the observed signals. It is also possible that multiple mechanisms compete with each other (see Section 5.4). A more detailed investigation of the root cause is needed in a follow-up study.

These findings confirm the indication that the fluffy (hollow) analog of the compact dust particle may produce a lower total impact charge yield (Section 4.2). Both effects, the increased charge yield and signal rise time for the compact particles compared to the fluffy (hollow) analog would result in an underestimated fluffy dust particle mass, if the detector were calibrated with compact dust particles. If the observed effect can be confirmed in future studies with improved dust analogs, the mass of previously detected fluffy ISD particles could have been underestimated by at least a factor of 2, based on the impact charge yield alone, at least for the larger (e.g. micron-sized) and potentially fluffy ISD

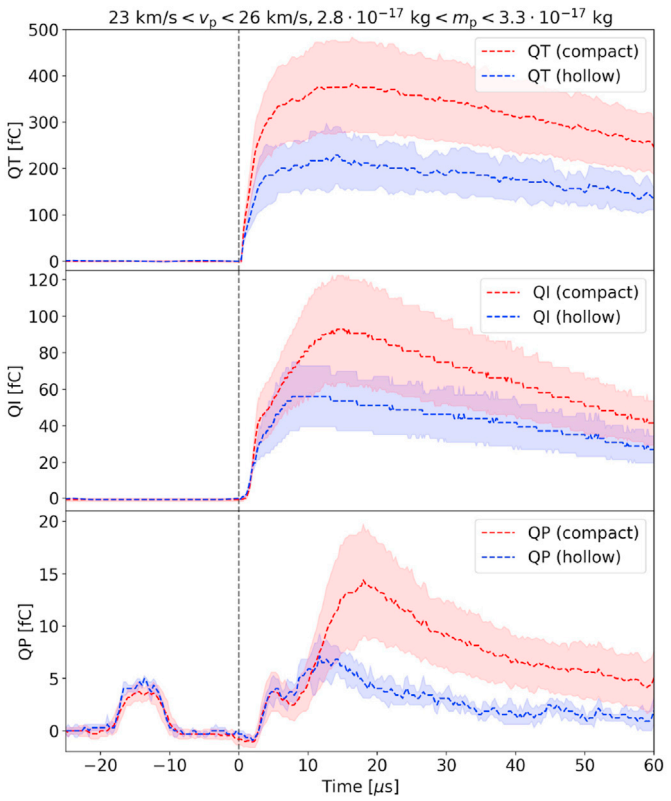

Fig. 16. Median QT, QI and QP signals from 108 to 11 IIT impacts of compact silicates from Batch II and hollow silicates, respectively, for a narrow range of dust masses m_p and impact velocities v_p. The filled areas around the signals indicate the spread of the data by showing the median absolute deviation of the different sets of signals that were used in the median. The impact time at $t = 0$ s is indicated by vertical dashed lines. Hollow particles of the same mass seem to generate less total impact charge.

particles detected by Ulysses (see (Strub et al., 2015; Sterken et al., 2015)).

It is important to note here that our result is based on only a small amount of the data, it is unsure if hollow spheres can be considered good fluffy analogs of compact dust particles and the densities of the hollow and compact particles were only 30% different. Also, if we compare the signals of a very limited amount of impact events from compact and hollow dust particles with similar velocities and masses (see Fig. 18 and 19 in Appendix E), we notice that the impacts of compact particles do not always produce more charge. Therefore, the observed differences could be dependent on particle mass and velocity, or the effect may not be significant enough to be detected in a single measurement.

5.4. Charge yield from carbon aerogel and compact iron particles

The impact charge yield from carbon aerogel particles is similar to iron particles (based on a small dataset), despite the different bulk density and composition. Several factors affect the ion generation process: on the one hand, the bulk density of the carbon aerogel is much lower than the iron (0.2 g/cm^3 compared to 7.8 g/cm^3) which may generate more ions from the dust particles upon impact (cf. the topic of this study). On the other hand, its ionization potential is slightly higher (11 keV compared to 8 keV) and there may be more secondary ions generated by the compact iron because of the secondary mechanism that is not yet well understood (we speculate on either more impact ejecta causing secondaries, or more ions from the target material, see also Sections 2 and 5.3). Comparisons of charge yields for such low density materials with compact particles of the same composition are needed to further study this topic and identify the dominating mechanisms.

6. Conclusions and outlook

6.1. Impact ionization of compact, hollow and fluffy dust

The dust accelerator experiments presented in this work indicate that it may be important to consider the dust particle structure and density for the interpretation of impact ionization experiments. We identified and compared impacts from dust particles with equal composition but different particle structures (i.e. single compact silicate spheres, clusters of silicate spheres and single hollow silicates spheres) and concluded as follows:

- Fluffy dust analogs can produce less impact charges (instead of more, as suggested in Section 1) than their compact counterparts.
- Our experiments indicate that a secondary process (we speculate on secondary impacts from ejecta or more target material ionization) could be the main cause for the observed differences. An increase in ionization of low-density dust with respect to compact dust may be compensated for, or overruled by this secondary process. Further investigations into the cause are necessary with improved dust analogs and compact particles of the same material.
- We speculate that, if confirmed by future experiments with larger statistics for various velocities (and compositions), the outgoing QP signal (or equivalent in future instruments) may be an indicator for porosity of the measured dust.
- Velocities of porous dust particles may be overestimated (if derived from the rise time), and their masses may be underestimated by current instrument calibrations with compact particles (see Section 6.2).

6.2. Consequences for in situ cosmic dust measurements

If the effect of dust porosity that we see in this study can be confirmed through new experiments with improved porous dust analogs, then porous interstellar dust particles may even have larger masses than derived so far from the Ulysses measurements. Hence, we conclude that dust porosity most likely cannot explain the discrepancy between the heavy ISD particles as measured in situ and the size-distribution as derived by classical astronomical observations. Hence, “heavy” particles of a few micrometer in size like those reported in Krüger et al. (2015) indeed exist.

We can estimate an order of magnitude for the error of a dust measurement for porous dust with CDA,[5] based on the case shown in Fig. 16. For this worst case scenario, we assume that a fluffy (hollow) silicate with a mass of $3 \cdot 10^{-17}$ kg hits CDA a velocity of about 25 km/s. The previous calibrations with iron particles (based on Srama (2009)) would overestimate the impact velocity by about a factor of 2.4, and underestimate the mass by about a factor of 450. Most of the error results from overestimating the particle velocity due to the erroneous signal rise time calibration. Assuming the impact velocity was determined correctly, the mass would still be underestimated by a factor of 2. If we instead apply the new calibrations for compact silicates from this paper (e.g. Fig. 13) to this contrived measurement of a fluffy silicate, the particle velocity would still be overestimated by at least a factory of 1.2, and the mass would be underestimated by at least a factor of 6.

This conclusion is in stark contrast with our hypothesis stated in Section 1 and may have an impact on the mass distribution of previous in situ ISD measurements. A shift towards larger masses would not alleviate but instead further increase the discrepancy between classical models of dust sizes in the ISM and in situ ISD measurements, and would decrease the gas-to-dust mass ratio as derived for in situ measurements in Krüger

[5] The ISD particles reported by Altobelli et al. (2016) were generally smaller than 300 nm, compact, and their minimum velocity was determined using the spectra from impact ionization.

et al. (2015). The results are also highly relevant for IDPs (e.g. dust emitted by Enceladus, cometary dust, etc.), which is thought to be fluffy in nature, and which was and will be measured in situ with impact ionization dust detectors.

6.3. Future studies

This study is a first step to investigate the effect of dust particle density and structure on the impact ionization and resulting spacecraft dust detector signals. It lays a foundation towards further understanding of the impact ionization process, further improvement of dust analogs, and improving the interpretation of in situ impact ionization dust detector data. The impact ionization process of hollow, porous or fluffy dust particles is not fully understood from this study, and follow-up studies are required with an attention to a few important points that we identify in this study:

- The highly porous dust analogs may have to have a much larger density difference to the compact particles than the 30% between the compact and hollow silicates in this work. This could allow to study if there is also an effect on the primary charges produced during the impact, instead of just the secondary charges.
- A more realistic particle structure for the fluffy analogs is needed than the hollow dust particles used in this study, in order to accurately simulate the structure of cosmic dust.
- For a good comparison with ISD measurements of micron-sized dust particles, it would be necessary to accelerate heavy dust particles ($\approx 10^{-15}$ kg) to velocities above 20 km/s. This is currently not possible with any linear electrostatic accelerator. However, the problem may be solved in the future by using a different method to accelerate dust particles, or by manufacturing dust particles that can more easily acquire higher surface charges at the same mass.
- Studies of mass spectra from compact and fluffy dust particles are needed to reveal more details about differences between the impact ionization processes (e.g. more target ionization), and also to reveal whether the structure or porosity has an effect on the composition determination.
- Our experiments allowed for a direct comparison of compact dust and fluffy dust analogs in a short range of impact velocities and particle masses, thus we cannot eliminate the possibility that our results may be velocity and mass dependent (e.g. see Appendix E). Future experiments should investigate if significant effects can be found in a larger range of impact velocities, and in the outgoing QP signal. For this, more statistics are needed, and thus improved porous dust analogs that do not form agglomerates or stick to the needle of the dust source in the accelerator.
- Different types of dust detectors (PVDF, Antenna measurements, Piezo, etc.) may have to be tested for dust particles with different densities and structure.

6.4. Future dust analog materials

Improved fluffy dust analogs may have to address the problem that more porous dust particles can be more prone to breaking apart while being accelerated or sticking to each other or to the laboratory equipment. These are material science problems that have to be solved, in order to design improved future experiments. Nano- and microparticle engineering and architecting might offer new promising prospects. Dust analogs can by manufactured synthetically with increasing precision, leveraging emerging materials synthesis capabilities. For example, gas-phase synthesis processes, such as flame spray pyrolysis give access to a wide variety of nanoparticles and fractal-like agglomerates with excellent control over particle size and composition. Metals, metal oxides and salts can be produced from metal organic precursor materials in a straightforward manner with accurate stoichiometric control (Athanassiou et al., 2010). The flame spray pyrolysis process is extremely versatile and scalable; tens of grams of samples can be produced in a small lab-scale reactor in a day (Gröhn et al., 2014). Flame-made silicate based materials, carbon/soot, iron oxides, or other ceramics might be promising fluffy dust candidate materials. Alternatively, the increasing ability of wet-phase chemistry to assemble nanoparticulate objects from molecular building blocks gives access to materials with tunable size, shape, composition and porosity, such as zeolites or organic/inorganic hybrid materials and lattices (Kaneti et al., 2017). For next generation dust analogs, we foresee that major synergies might arise from interdisciplinary collaborations between nanoparticle scientists and materials engineers and our community. However, with the increasing availability of candidate materials comes the choice of selecting the most promising ones. We thus also encourage interdisciplinary collaboration on the particle characterization front in order to define design specifications for dust analogs and to allow preselection of most promising candidates.

CRediT author statement

S. Hunziker: Methodology, Software, Formal analysis, Investigation, Data Curation, Writing - Original Draft, Writing - Review & Editing, Visualization, G. Moragas-Klostermeyer: Investigation, J. K. Hillier: Resources, Writing - Original Draft, L. A. Fielding: Resources, Writing - Original Draft, K. Hornung: Investigation, Writing - Original Draft, Writing - Review & Editing, J. R. Lovett: Resources, S. P. Armes: Resources, Writing - Original Draft, J. Fontanese: Resources, D. James: Resources, H.-W. Hsu: Investigation, I. Herrmann: Investigation, Writing - Original Draft,N. Fechler: Resources, O. Poch: Resources, A. Pommerol: Resources, R. Srama: Investigation, Writing - Review & Editing, D. Malaspina: Writing - Review & Editing, V.J. Sterken: Conceptualization, Formal analysis, Investigation, Data Curation, Writing - Original Draft, Writing - Review & Editing, Supervision, Project administration, Funding acquisition.

Declaration of competing interest

The authors declare that they have no known competing financial interests or personal relationships that could have appeared to influence the work reported in this paper.

Acknowledgments

The authors are grateful for 6 months of funding received from the Physics Department at the ETH Zürich for S. Hunziker. V.J. Sterken (VJS) received funding from the European Union's Horizon 2020 research and innovation programme under grant agreement N°851544. This work has been carried out within the framework of the NCCR PlanetS supported by the Swiss National Science Foundation under grants 51NF40_182901 and 51NF40 205606. Experimental design, preparation, work and preliminary data analysis were carried out while VJS worked for the University of Stuttgart and the International Space Science Institute. We thank Beatrice Frey, DCBP, University of Bern, for taking the SEM images shown in Figs. 1, 2, 4 and 5. We thank Daniela Fischer for the Laser particle size measurements performed at the Institute of Geography in Berne. We thank Prof. Mezger, from the Institute of Geological Sciences at the University of Bern for the support while preparing and characterizing the dust particles. Finally, we thank the anonymous referees for their helpful comments on the manuscript.

Appendix

A. Overview over previous experiments

Table 3
Overview of materials flown in previous impact ionization experiments, with reference.

Material	Size (μm)	Density (g/cm^3)	Coating	Target[a]	Impact vel. (km/s)	Reference
SiO_2	1–60	2	Zn	Ulysses/Galileo det.	2–30	Goeller and Gruen (1989)
Fe	0.6–30	7.9	–	Ulysses/Galileo det.	2–60	Goeller and Gruen (1989)
C	1.2–3.2	2.2	–	Ulysses/Galileo det.	4–30	Goeller and Gruen (1989)
Polystyrene	0.1–5	1.1	div. polymer[b]	Cu	0.2–35	Burchell et al. (1999a)
Fe	0.05–0.9	7.9	–	Au, Ag, In, Fe, Rh, Mo	2–80	Burchell et al. (1999b)
Polystyrene	0.2–1.8	1.1	PPy, PEDOT	CDA (CAT)	3–37	Goldsworthy et al. (2002, 2003)
PPy	0.1	1.5	–	CDA (CAT)	16–40	
AlSi	0.04–0.9	2.5	PPy	CDA (CAT)	3–51	Goldsworthy (2003)
Al	0.5–3	2.7	–	CDA (CAT)	2–55	Stübig (2002)
C	0.5	2.2	–	CDA (IIT + CAT)	2–30	Stübig (2002)
Fe	1	7.9	–	CDA (IIT + CAT)	2–70	Stübig (2002)
Polystyrene	0.75	1.1	Polyaniline	CDA (IIT + CAT)	4–25	Stübig (2002)
Polystyrene	1.6	1.1	PPy	CDA (IIT + CAT)	2–30	Stübig (2002)
Fe	0.08–2	7.9	–	Au	5–57	Mocker et al. (2013)
Orthopyroxene	0.14–2.6	3.5	Pt	Au	3–33	Mocker et al. (2013)
Olivine	0.05–0.4	3.4	PPy	Au, Fe, Cr	19–73	Mocker et al. (2013)
Fe	0.08–0.8	7.9	–	Rh	4–40	Mocker et al. (2013)
Orthopyroxene	0.1–4	3.5	Pt	CDA (CAT)	1.4–40	Fiege et al. (2014)
Fe	0.1–2	7.9	–	Ag, BeCu, Kapton, Solar cell, MLI[c]	2–40	Collette et al. (2014)

[a] Either the name of a dust analyzer instrument or the target material used in the experiment.
[b] PPy, PANi and PEDOT.
[c] Multilayer thermal insulation.

B. Dust analog coating process

Prior to coating with polypyrrole (PPy), the compact silicate particles were surface-modified with MPS according to a protocol previously described by Lovett et al. (2014). Briefly, compact silicate particles (1.30 g, theoretical mean diameter of 205 nm) were dispersed in deionized water (5.21 g) and vigorously stirred using a magnetic flea. This aqueous dispersion was heated to 70 °C and MPS (81 mg, target degree of functionalization = 10 MPS molecules per nm^2) was added using a micropipette. The reaction mixture was stirred vigorously for 5 h before being cooled to 20 °C.

The resulting MPS-treated silicate particles were then coated with a PPy overlayer using an aqueous deposition protocol previously described by Lovett et al. (2014) and summarized by Fielding et al. (2015). In each case, a mean PPy overlayer thickness of 10 nm was targeted using an estimated particle density and particle size data. In a typical protocol, the MPS-modified compact silicate particles were coated with PPy (19.0% w/w theoretical and 22.3% w/w PPy measured) by first adding pyrrole monomer (230 µl) using a micropipette. After 30 min, ammonium persulfate (0.81 g) was added and the aqueous dispersion was stirred at 20 °C for 3 h. The PPy-coated compact silicate particles were purified by filtration and then washed with deionized water and ethanol to remove spent oxidant and other impurities such as unreacted MPS. The particles were dried for several days in an oven at 40 °C. A PPy overlayer was deposited onto hollow silicate particles (26.0% w/w PPy theoretical and 28.7% w/w PPy measured) and silicate aerogel (0.2% w/w PPy) using a similar protocol.

C. Particle impact mass and velocity determination

For the study of the instrument response as a function of the impact parameters it is important to know the mass and velocity of the dust particle before the impact. This information is preferably reconstructed from the more precise charge and velocity measurements from either the Q_d instrument or the PSU since the QP signal is less sensitive to weakly charged particles and the velocity measurements are less precise. For this purpose, it is necessary to find for each impact registered by CDA the corresponding charge and velocity measurements in the Q_d and/or PSU data. This was not always straightforward because the clocks of the PSU experienced a drift, and because CDA only registers the impact time with a precision of 1 s. If either Q_d or PSU registered multiple dust particles per second, it may be impossible to reliably match a CDA impact to a corresponding charge and velocity measurement. For dust particles with a primary QP signal, however, the estimates for the particle charge and velocity from the QP signal can be used as additional criteria to find the corresponding dust particle in the Q_d and/or PSU measurements. For CDA impacts without primary QP signal there were often multiple possible matching Q_d/PSU events based on the impact time provided by CDA. However, if multiple possible matches were found, there are a few other criteria that can help deciding, which one of the Q_d/PSU measurements corresponds most likely to the CDA impact. Table 4 shows a summary of all criteria that were applied to find matching Q_d/PSU events and how they correspond to different classes that were defined to name the method used for finding matching pairs. For example, “Class 1” matches are CDA impact events with primary QP signal, for which a unique matching Q_d or PSU event could be found based on the impact time, and the charge and velocity estimates from the primary QP signal. For dust impacts without primary QP signal, we checked whether there was a unique Q_d/PSU measurement with matching impact time, a reasonable QI amplitude, a fitting velocity estimate from the QI rise time, or if one of the matching Q_d/PSU measurements had a surface charge that would have been below the detection limit of the QP detector. Classes 0, 11, 31, 52 and 62 designate CDA impacts for which no unique Q_d/PSU charge and velocity measurement could be identified, therefore such events had to be ignored in the data analysis. Some of the “Class 2” events had to be ignored in the data analysis as well because there were many obvious mismatches based on the impact time alone during times when the dust particle rate from the accelerator was particularly high. All other classes were used for the further data analysis in this work.

Table 4
Definition of the classes that indicate how the individual CDA impacts were matched to the Q_d and PSU measurements of the surface charge q and velocity v by using different matching criteria.

Class	primary	impact	matching q	matching v and	matching event below
	QP signal	time match	and QI amplitude	velocity from QI rise time	CDA detection limit
0	yes/no	none	–	–	–
1	yes	unique	–	–	–
11	yes	ambiguous	–	–	–
2	no	unique	–	–	–
3	no	ambiguous	unique	–	–
31	no	ambiguous	none	–	–
4	no	ambiguous	ambiguous	unique	–
51	no	ambiguous	ambiguous	ambiguous	unique
52	no	ambiguous	ambiguous	ambiguous	none/ambiguous
61	no	ambiguous	ambiguous	none	unique
62	no	ambiguous	ambiguous	none	none/ambiguous

D. Mass-Velocity distributions

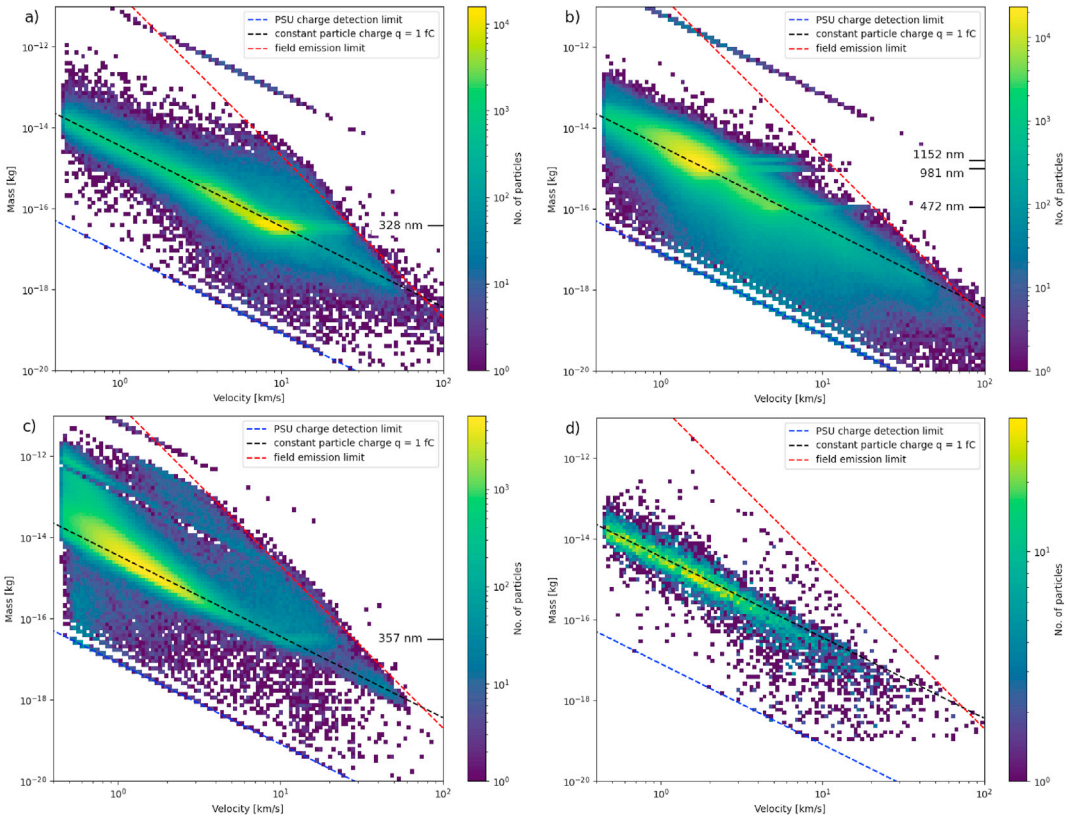

Fig. 17. Mass-velocity distributions of the dust particles provided by the dust source and measured by the PSU for (a) compact silicates from Batch II, (b) compact silicates from Batch I, (c) hollow silicates and (d) carbon aerogel. Horizontal lines on the right indicate the particle sizes that dominate the size distributions of the dust samples. The prominent lines above the field emission limit in (a), (b) and (c) are most likely artefacts from the charge measurement.

The mass-velocity distributions in Fig. 11 show all dust particles that were provided by the dust source and measured by the PSU for each dust type and all experiments that are considered in this work. The blue line at the bottom indicates the threshold of the charge detection at the PSU, which we determined to be about 0.002 fC by looking at the lowest provided charge measurements. The mass-velocity relation for particles with constant charge is $m \propto v^{-2}$ (see Eq. (1)). The red line at the top indicates the estimated upper limit for the maximum surface charge of the dust particles due to ion field emission, which scales roughly as $m \propto v^{-4}$ (e.g. Fechtig et al., 1978; Grün et al., 2001; Mocker et al., 2011). Most of the dust particles are concentrated around the black lines which shows that - independent on the dust type - the majority of the particles that left the accelerator had a charge of about 1 fC. The highly concentrated regions in Fig. 17(a) and (b) indicate the locations of single compact silicate particles. Therefore, we suggest that the horizontal regions with higher concentration that originate from these regions are associated to single compact silicates that exhibited a larger than average charge, and were therefore accelerated to a higher velocity for the same particle mass. The number of such horizontal regions confirms the monodispersity of the sample of compact silicates from Batch II (Fig. 17(a)) and hollow silicates (Fig. 17(c)), and indicates that the compact silicates from Batch I (Fig. 17(b)) were comprised of particles with three different sizes. Furthermore, the majority the hollow silicates (Fig. 17(c)) must have been comprised of massive particle clusters. The carbon aerogel dust (Fig. 17(d)) consisted of a broader size distribution, and therefore does not show any of the aforementioned features.

E. Comparison of individual impact signals

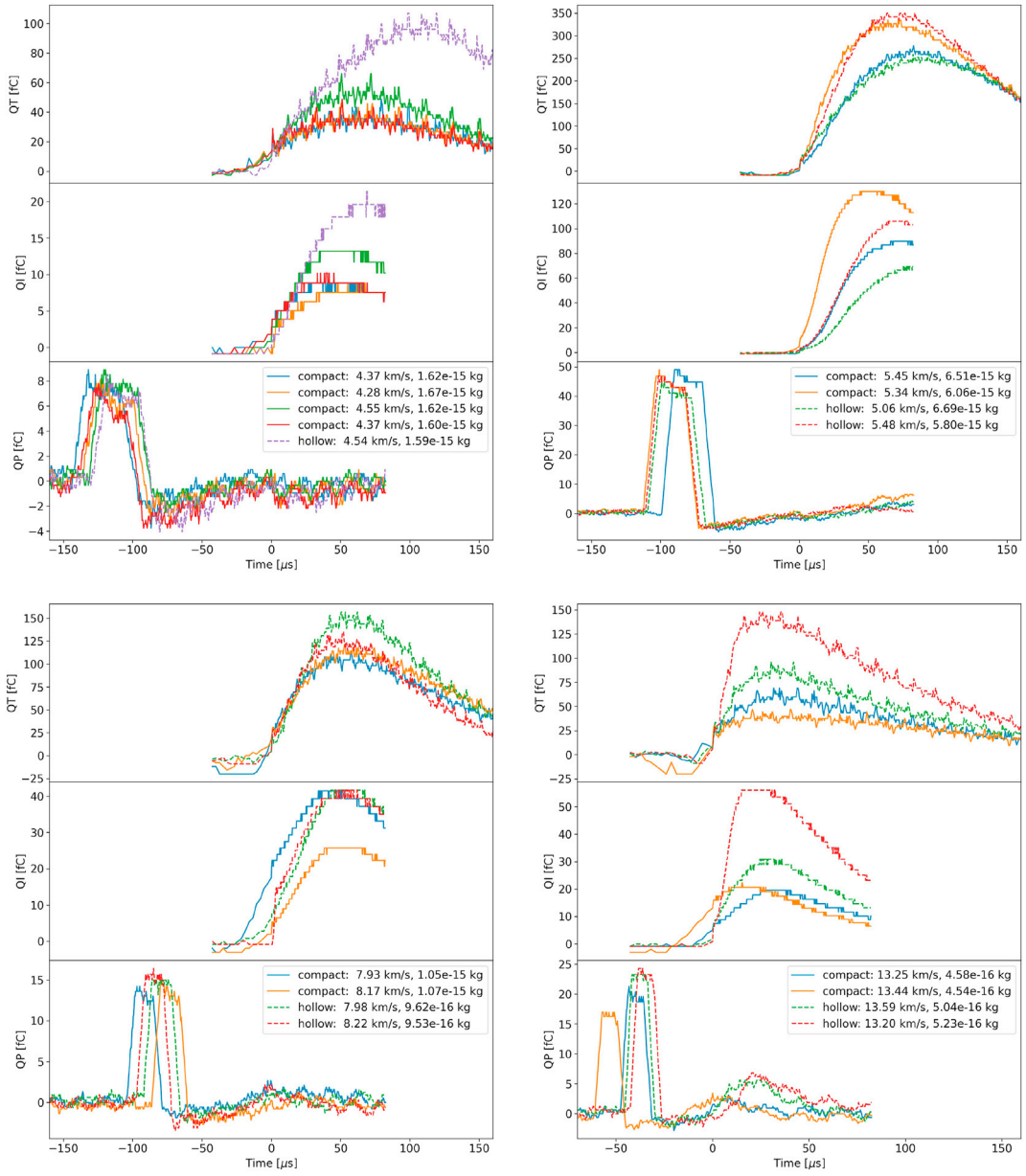

Fig. 18. QT, QI and QP signals from a number of IIT impacts of compact (Batch II) and hollow silicate dust particles. Each panel shows a few impacts from particles with similar masses and impact velocities for impact velocities between about 4 and 13 km/s.

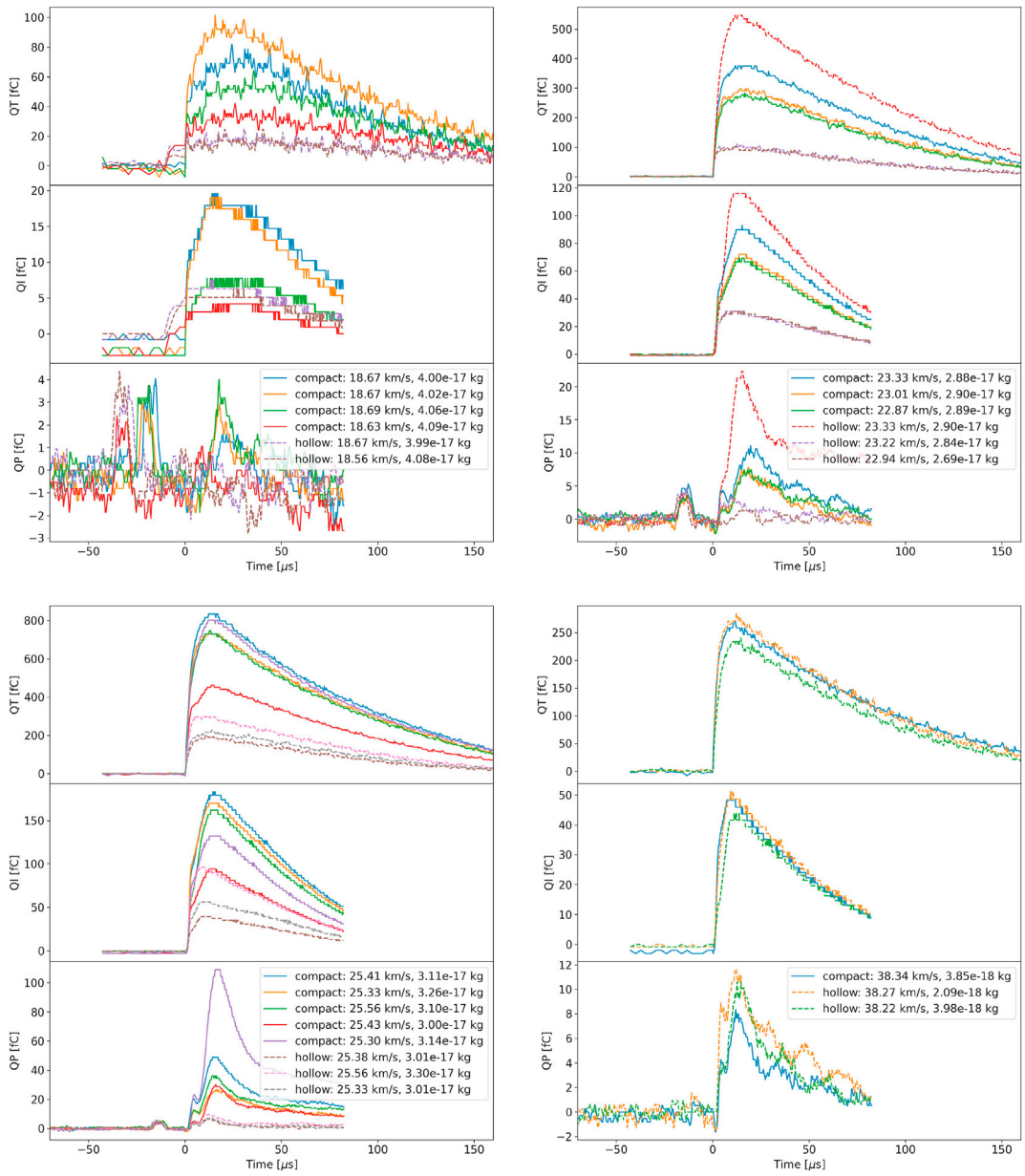

Fig. 19. QT, QI and QP signals from a number of IIT impacts of compact (Batch II) and hollow silicate dust particles. Each panel shows a few impacts from particles with similar masses and impact velocities for impact velocities between about 19 and 38 km/s.

References

Altobelli, N., Postberg, F., Fiege, K., et al., 2016. Science 352, 312. https://doi.org/10.1126/science.aac6397.

Athanassiou, E.K., Grass, R.N., Stark, W.J., 2010. Aerosol. Sci. Technol. 44, 161. https://doi.org/10.1080/02786820903449665.

Auer, S., 1994. In: Particle Capture, Recovery and Velocity/Trajectory Measurement Technologies. M. E. Zolensky, p. 21.

Auer, S., 2001. In: Interplanetary Dust, p. 385.

Auer, S., Grün, E., Srama, R., Kempf, S., Auer, R., 2002. planet 50, 773. https://doi.org/10.1016/S0032-0633(02)00019-3.

Bradley, J.P., Brownlee, D.E., 1986. Science 231, 1542. https://doi.org/10.1126/science.231.4745.1542.

Burchell, M.J., Cole, M.J., Lascelles, S.F., et al., 1999a. J. Phys. D Appl. Phys. 32, 1719. https://doi.org/10.1088/0022-3727/32/14/325.

Burchell, M.J., Cole, M.J., McDonnell, J.A.M., Zarnecki, J.C., 1999b. Meas. Sci. Technol. 10, 41. https://doi.org/10.1088/0957-0233/10/1/011.

Collette, A., Grün, E., Malaspina, D., Sternovsky, Z., 2014. J. Geophys. Res. 119, 6019. https://doi.org/10.1002/2014JA020042.

Dietzel, H., Eichhorn, G., Fechtig, H., et al., 1973. J. Phys. Scientific. Instrument. 6, 209. https://doi.org/10.1088/0022-3735/6/3/008.

Draine, B.T., 2009. SSRv 143, 333. https://doi.org/10.1007/s11214-008-9411-7.

Drapatz, S., Michel, K.W., 1974. Zeitschrift Naturforschung Teil A 29, 870. https://doi.org/10.1515/zna-1974-0606.

Fechtig, H., Gruen, E., Kissel, J., 1978. In: McDonnell, J.A.M. (Ed.), Cosmic Dust. Wiley, pp. 607–669.

Fiege, K., Trieloff, M., Hillier, J.K., et al., 2014. Icarus 241, 336. https://doi.org/10.1016/j.icarus.2014.07.015.

Fielding, L.A., Hillier, J.K., Burchell, M.J., Armes, S.P., 2015. Chem. Commun. 51, 16886. https://doi.org/10.1039/C5CC07405C.

Gall, C., Hjorth, J., 2018. APJ (Acta Pathol. Jpn.) 868, 62. https://doi.org/10.3847/1538-4357/aae520.

Gall, C., Hjorth, J., Watson, D., et al., 2014. Nature 511, 326. https://doi.org/10.1038/nature13558.

Gao, P., Kopparla, P., Zhang, X., Ingersoll, A.P., 2016. Icarus 264, 227. https://doi.org/10.1016/j.icarus.2015.09.030.

Goeller, J.R., Gruen, E., 1989. Planets 37, 1197. https://doi.org/10.1016/0032-0633(89)90014-7.

Goeller, J.R., Gruen, E., Maas, D., 1986. In: Battrick, B., Rolfe, E.J., Reinhard, R. (Eds.), ESA Special Publication, vol. 250. ESLAB Symposium on the Exploration of Halley's Comet, pp. 333–336.

Goldsworthy, B.J., Burchell, M.J., Cole, M.J., et al., 2002. Adv. Space Res. 29, 1139. https://doi.org/10.1016/S0273-1177(02)00129-1.
Goldsworthy, B.J., 2003. A&A 409, 1151. https://doi.org/10.1051/0004-6361:20031087.
Gröhn, A.J., Pratsinis, S.E., Sánchez-Ferrer, A., Mezzenga, R., Wegner, K., 2014. Ind. Eng. Chem. Res. 53, 10734. https://doi.org/10.1021/ie501709s.
Grün, E., Gustafson, B.A.S., Dermott, S., Fechtig, H., 2001. Interplanetary Dust. Springer.
Grün, E., Krüger, H., Srama, R., 2019. SSRv 215, 46. https://doi.org/10.1007/s11214-019-0610-1.
Grün, E., Zook, H.A., Baguhl, M., et al., 1993. Nature 362, 428. https://doi.org/10.1038/362428a0.
Güttler, C., Mannel, T., Rotundi, A., et al., 2019. A&A 630, A24. https://doi.org/10.1051/0004-6361/201834751.
Hah, H.J., Kim, J.S., Jeon, B.J., Koo, S.M., Lee, Y.E., 2003. Chem. Commun. 1712. https://doi.org/10.1039/B301521A.
Hillier, J.K., Sestak, S., Green, S.F., et al., 2009. Planets 57, 2081. https://doi.org/10.1016/j.pss.2009.09.019.
Hornung, K., Drapatz, S., 1981. In: ESA Special Publication, vol. 155. The Comet Halley Probe. Plasma Environment, p. 23.
Janisch, T., 2021. M.sc. Thesis. Eidgenössische Technische Hochschule Zürich.
Kaneti, Y., Tang, J., Salunkhe, R., et al., 2017. Adv. Mater. 29. https://doi.org/10.1002/adma.201604898.
Kempf, S., Srama, R., Graps, A., 2012. The Cosmic Dust Analyser Data Handbook.
Kissel, J., Krueger, F.R., 1987. Appl. Phys. Mater. Sci. Process 42, 69. https://doi.org/10.1007/BF00618161.
Krüger, H., Strub, P., Grün, E., Sterken, V., 2015. J. APJ (Acta Pathol. Jpn.) 812, 139. https://doi.org/10.1088/0004-637X/812/2/139.
Landgraf, M., 2000. J. Geophys. Res. 105, 10303. https://doi.org/10.1029/1999JA900243.
Landgraf, M., Baggaley, W.J., Grün, E., Krüger, H., Linkert, G., 2000. J. Geophys. Res. 105, 10343. https://doi.org/10.1029/1999JA900359.
Landgraf, M., Krüger, H., Altobelli, N., Grün, E., 2003. J. Geophys. Res. 108, 8030. https://doi.org/10.1029/2003JA009872.
Love, S.G., Joswiak, D.J., Brownlee, D.E., 1994. Icarus 111, 227. https://doi.org/10.1006/icar.1994.1142.
Lovett, J.R., Fielding, L.A., Armes, S.P., Buxton, R., 2014. Adv. Funct. Mater. 24, 1290. https://doi.org/10.1002/adfm.201302261.
Mannel, T., Bentley, M.S., Boakes, P.D., et al., 2019. A&A 630, A26. https://doi.org/10.1051/0004-6361/201834851.
Mathis, J.S., Rumpl, W., Nordsieck, K.H., 1977. APJ (Acta Pathol. Jpn.) 217, 425. https://doi.org/10.1086/155591.
Mocker, A., Bugiel, S., Auer, S., et al., 2011. Rev. Sci. Instrum. 82, 095111. https://doi.org/10.1063/1.3637461.
Mocker, A., Hornung, K., Grün, E., et al., 2013. Planets 89, 47. https://doi.org/10.1016/j.pss.2013.07.013.
Ratcliff, P.R., Burchell, M.J., Cole, M.J., Murphy, T.W., Alladfadi, F., 1997. Int. J. Impact Eng. 20, 663. https://doi.org/10.1016/S0734-743X(97)87453-2.
Ratcliff, P.R., Gogu, F., Grün, E., Srama, R., 1996. Adv. Space Res. 17, 111.
Rietmeijer, F.J.M., 1993. Earth Planet Sci. Lett. 117, 609. https://doi.org/10.1016/0012-821X(93)90106-J.
Srama, R., 2009. Habilitation. Universität Stuttgart.
Srama, R., Ahrens, T.J., Altobelli, N., et al., 2004. SSRv 114, 465. https://doi.org/10.1007/s11214-004-1435-z.
Sterken, V.J., Altobelli, N., Kempf, S., et al., 2012. A&A 538, A102. https://doi.org/10.1051/0004-6361/201117119.
Sterken, V.J., Strub, P., Krüger, H., von Steiger, R., Frisch, P., 2015. APJ (Acta Pathol. Jpn.) 812, 141. https://doi.org/10.1088/0004-637X/812/2/141.
Strub, P., Krüger, H., Sterken, V., 2015. J. APJ (Acta Pathol. Jpn.) 812, 140. https://doi.org/10.1088/0004-637X/812/2/140.
Stübig, M., 2002. Dissertation. University of Heidelberg.
Wang, S., Li, A., Jiang, B.W., 2015. APJ (Acta Pathol. Jpn.) 811, 38. https://doi.org/10.1088/0004-637X/811/1/38.
Weingartner, J.C., Draine, B.T., 2001. APJ (Acta Pathol. Jpn.) 548, 296. https://doi.org/10.1086/318651.
Westphal, A.J., Stroud, R.M., Bechtel, H.A., et al., 2014. Science 345, 786. https://doi.org/10.1126/science.1252496.
Zel'dovich, Y.B., Raizer, Y.P., 1967. Physics of Shock Waves and High-Temperature Hydrodynamic Phenomena.